Localised corrosion of heat-treated alloys Part II – Predicting grain boundary microchemistry and its effect on repassivation potential

A. Anderko*[1], N. Sridhar[2] and G. Tormoen[3]

A methodology has been developed for predicting the effect of thermal aging on the repassivation potential of austenitic alloys. The methodology combines two models, a grain boundary microchemistry model for calculating the chromium and molybdenum depletion profiles in the vicinity of grain boundaries and an electrochemical model that relates the repassivation potential to the microchemistry and environmental conditions, including temperature and solution chemistry. The grain boundary microchemistry model incorporates a thermodynamic paraequilibrium treatment of the formation of carbides and a kinetic treatment of the diffusion of Cr and Mo. With this model, experimental Cr and Mo depletion profiles can be reproduced for sensitised alloys 600, 825 and 316L. The repassivation potential model accounts for the effects of solution chemistry and temperature by considering competitive dissolution, adsorption and oxide formation processes at the interface between the metal and the occluded site solution. Using a previously developed relationship between the repassivation potential and bulk alloy composition, a procedure has been established for calculating the observable repassivation potential of thermally aged alloys by integrating the local E_{rp} values that correspond to the alloy microchemistry in the depletion zone. The predicted repassivation potentials agree with experimental data for thermally aged alloys 600 and 825 in chloride solutions. Additionally, the model has been applied to estimate the repassivation potential of welded samples in which segregation of alloying elements is observed.

Keywords: Localised corrosion, Alloys 600, 825 and 22, Repassivation potential, Thermal aging

Introduction

Localised corrosion of engineering alloys is a complex function of metallurgical factors and environmental conditions. Among metallurgical factors, effects of thermal instabilities are of interest for assessing the performance and expected service life of industrial components fabricated from nominally corrosion-resistant stainless steels and nickel-based alloys. Fabrication processes such as heat treatment and welding are known to introduce microstructural changes that may affect both the mechanical and corrosion performance of an alloy. In particular, thermal instability of stainless steels and nickel-based alloys may lead to the formation of complex metal carbides of the type M_3C_2, M_7C_3, M_6C or $M_{23}C_6$ in which the metallic component M represents Cr, Mo, W and Fe. The carbide is chromium- or molybdenum-rich depending on the carbide type, which in turn depends on the alloy composition and temperature. In addition, chromium-rich intermetallic phases such as the σ, χ, R and μ phases can form in many alloys.[1,2] Precipitation of such phases may occur at temperatures ranging from 500 to 900°C depending on alloy composition. Formation of grain boundary carbides often results in the depletion of chromium and possibly, molybdenum in the vicinity of the grain boundary because of the slow diffusion of substitutional elements such as chromium relative to the interstitial carbon. Similarly, the corrosion resistance of welded components may be affected by the segregation of alloying elements and precipitation of intermetallic phases, carbides or nitrides in the solidified weld and unmixed zones as well as the precipitation of carbides and other phases in the heat-affected zone adjacent to the weld.[3]

Sensitisation of Fe–Ni–Cr–Mo alloys and its effects on intergranular attack (IGA) and intergranular stress

[1]OLI Systems Inc, 108 American Road, Morris Plains, NJ 07950, USA
[2]Det Norske Veritas, 5777 Frantz Road, Dublin, OH 43017, USA
[3]Southwest Research Institute, Department of Materials Engineering, 6220 Culebra Road, San Antonio, TX 78238, USA

*Corresponding author, email aanderko@olisystems.com

Published by Maney on behalf of the Institute
Received 14 May 2008; accepted 10 April 2009
DOI 10.1179/174327809X409240

corrosion cracking (IGSCC) has been extensively modelled in the literature.[4–13] Much less effort has been devoted to pitting and crevice corrosion of thermally aged and fabricated alloys. Most of the studies of localised corrosion of thermally aged or welded stainless steels and Ni-based alloys have been focused on developing comparative performance data in specific environments, for example, critical crevice temperatures in ferric chloride solutions. Recent localised corrosion studies have been focused on characterising the dependence of localised corrosion parameters in certain environments on thermal aging of Ni-based alloys, i.e. alloy 825[14] and alloy 22.[15–17] In the first part of this study,[18] the authors investigated the localised corrosion of alloy 600. However, no generalised treatment has been proposed so far to rationalise and predict the effects of heat treatment on the susceptibility of Fe–Ni–Cr–Mo alloys to pitting or crevice corrosion.

In the authors' previous papers,[19,20] a computational methodology has been proposed to predict the tendency of base metals to undergo localised corrosion. This methodology is based on the computation of two characteristic parameters as functions of aqueous environment composition and temperature, i.e. the corrosion potential E_{corr} and the repassivation potential E_{rp}, also called the protection potential. The repassivation potential provides a threshold condition below which stable pitting or crevice corrosion does not occur.[19,21,22] E_{rp} is amenable to modelling because it is relatively insensitive to surface finish and coincides for pitting and crevice corrosion as long as propagation exceeds a certain minimum value.[22] The values of E_{rp} and E_{corr}, calculated as a function of environmental conditions, can be then compared to determine the susceptibility of an alloy to localised corrosion.[20,22] To predict the repassivation potential as a function of environmental conditions, a mechanistic model was developed in a previous paper.[19] This model was shown to reproduce E_{rp} for a number of alloys in laboratory solutions and in complex chemical process environments.[23] The repassivation potential model can be used as a predictive tool for alloys in multicomponent industrial environments because its parameters are expressed as functions of aqueous solution chemistry. Moreover, the E_{rp} model parameters have been correlated with the composition of Fe–Ni–Cr–Mo–W–N alloys,[24] thus making it possible to predict the effect of compositional variations in an alloy on E_{rp}.

The objective of this study is to find a quantitative relationship between the repassivation potential and the microstructural changes that are associated with thermal instabilities. For this purpose, the authors establish a new model for predicting the chromium and molybdenum depletion profiles that develop at grain boundaries as a result of sensitisation. Then, the authors combine the new grain boundary chemistry model with the previously developed repassivation potential model to predict E_{rp} of thermally aged alloys or alloys with compositional changes due to element segregation during solidification. This allows us to establish a link between the microstructural variations in alloy composition and the observable, macroscopic values of the repassivation potential, thus providing a threshold condition for localised corrosion. Furthermore, the predictions are verified using previously obtained repassivation potential data for thermally aged alloys 600 and 825 and welded alloy 22.

Experimental

The modelling studies reported here rely on the previous experimental results of Tormoen *et al.*[18] and Pan *et al.*[14] for the repassivation potential of heat-treated alloys 600 and 825 respectively. In addition, the authors use the repassivation potential data reported by Dunn *et al.*[15–17] for welded samples of alloy 22. The nominal compositions of the alloys studied here are summarised in Table 1. In addition to the repassivation potential data, depletion profile data for alloys 600, 825 and 316L are used to verify the grain boundary composition model. The sources of these data are listed in Table 2.

Computational model

The computational model developed in this study consists of three parts, i.e.

(i) a grain boundary microchemistry model for predicting the chromium and molybdenum depletion in the vicinity of grain boundaries as a result of carbide formation
(ii) an electrochemical model for calculating the repassivation potential of Fe–Ni–Cr–Mo–W alloys as a function of alloy composition and environmental conditions including temperature and concentrations of aqueous solution species
(iii) a procedure for calculating the observable repassivation potential that corresponds to macroscopic localised corrosion by applying the electrochemical model to the depletion profiles and performing suitable integration.

Grain boundary microchemistry model

Review of literature models

In the last four decades, several computational models have been developed to predict the redistribution of alloying elements in the vicinity of grain boundaries.[4,10,11,13,25–31] The motivation for these studies was to be able to understand and quantitatively predict IGA and IGSCC, which are controlled by the depletion of chromium in a region adjacent to the grain boundary. The models developed in the literature can be roughly divided into two classes, i.e.

(i) models that combine a thermodynamic equilibrium formalism for metal carbide formation with a kinetic treatment of the redistribution of Cr and other elements as a function of the distance from the grain boundary[4,10,11,25,26,28,30]
(ii) models that rely on a kinetic treatment of the evolution of grain boundary chromium

Table 1 Nominal compositions of alloys studied

		Nominal composition, wt-%					
Alloy	UNS no.	Ni	Fe	Cr	Mo	C	Other
600	N06600	Bal.	8·0	15·5	0	0·02 (lot 1) 0·04 (lot 2)	
825	N08825	Bal.	33·5	21·5	3·0	0·01	Cu=2
316L	S31603	10·0	Bal.	17·0	2·5	0·03 (max)	
C-22*	N06022	Bal.	3·0	22·0	13·0	0·01	W=3

*Registered trademark of Haynes International.

concentration without explicitly invoking thermodynamic relationships for the local equilibrium associated with carbide formation.[13,29,31] Such an approach can be used to facilitate separating the stages of chromium depletion and self-healing[29] or to introduce a detailed, three-dimensional treatment of the growth kinetics of carbides.[31]

The literature models have been successful in predicting the Cr depletion profiles[10,11,13,29] and the critical conditions of sensitisation as investigated using electrochemical potentiokinetic reactivation[28] and IGA/IGCC susceptibility data.[11,13] Much less attention has been devoted to molybdenum depletion, primarily because Mo depletion data are much less abundant in the literature. However, the computation of Mo depletion profiles is of great interest here because of the importance of Mo in localised corrosion.

Requirements for microchemistry model

In this study, the authors develop a grain boundary microchemistry model that serves as a foundation for predicting the effect of heat treatment on localised corrosion. While the concepts introduced in the combined thermodynamic/kinetic models mentioned above are utilised, the authors construct the model in a way that is particularly suitable for applications to localised corrosion prediction. For this purpose, the model is designed to satisfy the following requirements:

(i) it should be applicable to the prediction of Mo depletion as well as Cr depletion as a function of temperature and time of heat exposure

(ii) it should make it possible to predict the effects of variations in bulk alloy composition and, in particular, the alloy's carbon content rather than merely fit the depletion profiles for individual alloys. This requirement necessitates the use of a thermodynamic model for the alloy phase

(iii) the model parameters should be limited to quantities that have a well-defined physical meaning, can be obtained from independent experimental data or reasonably estimated and are readily transferable to similar alloys. This requirement effectively limits the model to the use of thermodynamic functions of formation of carbides, thermodynamic parameters for activity coefficients in solid solutions, diffusion coefficients and the average grain size

(iv) the computations should be reasonably fast because they need to be performed numerous times. This means that the authors endeavour to develop analytical expressions, whenever possible, rather than numerically solving the pertinent diffusion equations. Therefore, multicomponent diffusion effects[30] are not taken into account and diffusion equations are written in terms of concentrations of individual alloy components.

Compared with the models described in the open literature, the key new features of the proposed model are

(i) computation of the full time evolution of alloying element depletion (including healing) using easily solvable algebraic equations that incorporate the thermodynamic, diffusion and mass balance aspects of the phenomenon (rather than having to solve differential equations numerically)

(ii) a simple, yet accurate method for predicting Mo depletion together with Cr depletion. This will be achieved without using any empirical parameters beyond those specified in requirement (iii) above.

Assumptions for modelling grain boundary chemistry

To develop a simple model for calculating the depletion profiles as a function of temperature and time of heat exposure and bulk alloy composition, the authors adopt the following assumptions:

(i) the precipitating carbides can be treated as if they form a grain boundary film of equivalent, averaged thickness and consequently, the diffusion in the matrix can be treated as one-dimensional. Grain boundary diffusion can be assumed to be sufficiently rapid to establish equilibrium along the grain boundaries between carbide particles and the adjacent region of the matrix. In reality, grain boundary precipitates are

Table 2 Parameters of grain boundary chemistry model, average deviations from experimental data and sources of depletion profile data

	Parameters for carbides				Diffusion coefficients						
Alloy	Stoichiometry	Mo/Cr ratio	A, kJ mol^{-1}	B [J mol^{-1} K^{-1}]	D^0_{Cr} (m^2/s)	Q_{Cr} (kJ/mol)	D^0_{Mo} m^2 s^{-1}	Q_{Mo}, kJ mol^{-1}	Grain size g, μm	Average deviation*	Data source
600	M_7C_3	0	−405·2	−25·77	$4{\cdot}40\times10^{-4}$	−243	n/a	n/a	123	0·0052	10
									82	0·0097	39
									37	0·0074	8
825	$M_{23}C_6$	0·078	465·7	−1400	$1{\cdot}68\times10^{-4}$	−287	$7{\cdot}93\times10^{-5}$	−274	160	0·0127	14
316L	$M_{23}C_6$	0·165	41·22	−966	$1{\cdot}68\times10^{-4}$	−289	$7{\cdot}93\times10^{-5}$	−274	253	0·0139 (Cr) 0·0009 (Mo)	45
									138	0·0071	46, Krupp sample
									30	0·0055	46, Creusot–Loire sample
									30	0·0055 (Cr) 0·0056 (Mo)	7

*The average deviation is defined as $\mathrm{AAD}=\frac{1}{N}\sum_{i}^{N}\left|x_i^{cal}-x_i^{exp}\right|$ where N is the number of experimental points and xi are the mole fractions of Cr or Mo.

often discontinuous, a fact that is used in measuring grain boundary depletion profiles without interference from the carbides. However, for model simplification, the authors assume that these discontinuous particles can be treated as if they coat the grain boundaries uniformly

(ii) since the interstitial diffusion of carbon is several orders of magnitude faster than the diffusion of substitutional elements (i.e. Cr, Mo, Ni and Fe), carbon activity can be assumed to be equal throughout the material

(iii) at the carbide/matrix interface, local thermodynamic equilibrium (or paraequilibrium) is assumed. This equilibrium is determined by the local activity of Cr and Mo and the global activity of C

(iv) at a sufficiently long distance from the grain boundary, the concentrations of substitutional elements are the same as those in the bulk alloy because the amount of these elements precipitated as carbides is small compared to their original amounts. On the other hand, the concentration of carbon decreases appreciably as the process of carbide formation advances

(v) the carbides may be of the form M_7C_3 or $M_{23}C_6$ and contain only Cr and, if applicable, Mo in addition to carbon. While the authors do not consider other carbide phase compositions in this study, an extension of the model to other stoichiometries would be straightforward

(vi) carbide nucleation and incubation time are neglected, and the model deals only with the growth of the carbides

(vii) carbide growth is controlled by the diffusion of the metallic component of the carbide. The diffusion coefficients are independent of concentration

(viii) the moving boundary at the carbide/matrix interface is ignored in diffusion calculations. This implies that the thickness of the carbide is negligible in comparison to the grain diameter.

For simplicity, the authors first describe the computation of chromium depletion profiles and then present its extension to treat molybdenum depletion.

Derivation of semi-analytical model of Cr depletion

Figure 1 defines the variables used in the microchemistry model and presents a scheme of material balances for Cr and C in the carbide and alloy phases. The essential features of this scheme were first introduced by Zener[32] and have been generally adopted in physical metallurgy.[33] The authors assume that the concentrations of Cr in the bulk alloy and in the carbide phase β are C^0_{Cr} and C^{β}_{Cr} respectively. As in the previously published models,[10,11,13,27–30] it can be assumed that the bulk concentration C^0_{Cr} remains practically unchanged. This assumption can be easily verified by calculating the maximum possible drop in bulk Cr concentration that would be obtained in the hypothetical case if all carbon in the alloy was incorporated into the carbide phase. For the alloys listed in Table 1, such a calculation yields a drop of the order of 1%, which is within the uncertainty of depletion profile measurements. The concentration of Cr at the matrix (γ)/carbide (β) interface is given by $C^{\gamma\beta}_{Cr}$ and results from the paraequilibrium between the carbide phase and chromium and carbon from the matrix. At a given instant of time t, the carbide thickness is r and the concentration of Cr in the matrix is a function of the distance from the grain boundary z and is given by the function $C^{\gamma}_{Cr}(z)$. The area of the rectangle U represents the accumulation of Cr in the carbide at a given instant of time. The consumption of chromium as a result of carbide growth is balanced by the diffusion of Cr from the bulk, which results in a Cr concentration gradient as given by $C^{\gamma}_{Cr}(z)$. Thus, the area U is always equal to the chromium content that has been withdrawn from the depleted zone V.[4,13] The mass balance for chromium (Fig. 1, upper diagram) is inextricably linked with the mass balance for carbon (Fig. 1, lower diagram). Simultaneously with the accumulation of Cr within the carbide, carbon is progressively consumed,

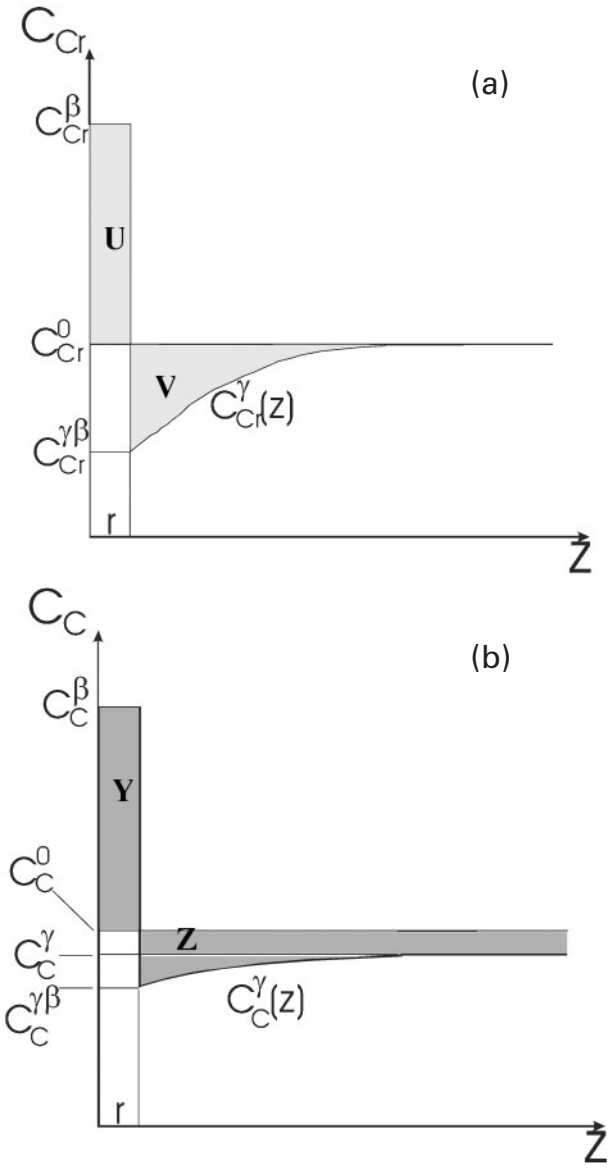

1 Scheme of grain boundary material balance calculations for Cr *a* and C *b*. Concentrations of Cr and C and denoted by C_{Cr} and C_C respectively. Superscripts 0, β, γ and $\gamma\beta$ denote concentrations in original alloy, carbide phase, bulk alloy and at alloy–carbide boundary respectively. The distance from the grain boundary is denoted by *z*, and *r* is dimension of grain boundary precipitate

and its concentration drops throughout the grain. While the activity of carbon remains constant within the grain, its concentration develops a certain profile in the vicinity of the grain boundary as a function of z (cf. $C_C^{\gamma}(z)$ in Fig. 1, lower diagram) because the activity coefficient of carbon varies with the changing concentration of Cr and other elements. The drop in the matrix concentration of carbon (i.e. from the original concentration of C_C^0 to C_C^{γ}) entails a drop in the interface concentration to $C_C^{\gamma\beta}$ until the matrix carbon concentration reaches the solubility limit. The interface concentrations of carbon $C_C^{\gamma\beta}$ and chromium $C_{Cr}^{\gamma\beta}$ are linked through the thermodynamic equilibrium of carbide formation

$$v_{Cr}Cr + v_C C = Cr_{v_{Cr}}C_{v_C} \tag{1}$$

where v_{Cr} and v_C are the stoichiometric coefficients of chromium and carbon within the carbide respectively.

Thus, the growth of the carbide and the corresponding evolution of the concentration profiles are controlled by the flow of carbon as well as chromium to the interface. Since the available amount of carbon is finite within a grain, the depletion profile will depend on the grain size, which determines the available volume from which carbon can be withdrawn to form the carbide. The conservation of mass requires that the areas Y and Z in Fig. 1 (lower diagram) be equal to each other because the carbon content in the carbide Y is equal to the amount of carbon withdrawn from the matrix Z. The model must simultaneously satisfy the two mass balance conditions, i.e. $U=V$ and $Y=Z$.

Since the model is assumed to be one-dimensional, the chromium concentration profile can be obtained from Fick's second law, i.e.

$$\frac{\partial C_{Cr}}{\partial t} = D_{Cr}\frac{\partial^2 C_{Cr}}{\partial z^2} \tag{2}$$

where D_{Cr} is the diffusion coefficient of Cr. The concentration profile can be expressed as a function of time t and distance from the grain boundary z using the error function solution[13,34]

$$C_{Cr}^{\gamma}(z,t) = C_{Cr}^{\gamma\beta} + (C_{Cr}^0 - C_{Cr}^{\gamma\beta})\mathrm{erf}\left[\frac{z}{2(D_{Cr}t)^{1/2}}\right] \tag{3}$$

where the superscripts denote the phases and have been explained in Fig. 1. Since the concentration of component i C_i is related to its mole fraction x_i and molar volume of the matrix V_m by

$$C_i = \frac{x_i}{V_m} \quad (i = \mathrm{Cr, Fe, Ni, C, \ldots}) \tag{4}$$

Equation (2) can be rewritten in a more convenient form by using mole fractions, i.e.

$$x_{Cr}^{\gamma}(z,t) = x_{Cr}^{\gamma\beta} + (x_{Cr}^0 - x_{Cr}^{\gamma\beta})\mathrm{erf}\left[\frac{z}{2(D_{Cr}t)^{1/2}}\right] \tag{5}$$

The accumulation of Cr in the carbide phase, as depicted by area U in Fig. 1, is given by

$$\Delta n_{Cr}^{\beta} = (C_{Cr}^{\beta} - C_{Cr}^0)S\bar{r} \tag{6}$$

where S is the surface area of the grain, and $\bar{r}$ is the average thickness of the carbide phase along the z axis. The parameter $\bar{r}$ should be regarded as a statistical average and, in actuality, reflects the total volume of the carbide phase (when multiplied by S). Therefore, it does not necessarily represent the actual dimension of the carbide and is equally applicable to continuous and discontinuous intergranular carbides. It is introduced in order to calculate the mass balances of Cr and C because the same volume of the carbide phase is available to both Cr and C. The total depletion of Cr in the grain can be calculated by integrating the local depletion over the entire grain, i.e.

$$\Delta n_{Cr}^{\gamma} = S\int_0^{\infty}\left[C_{Cr}^0 - C_{Cr}^{\gamma}(z,t)\right]\mathrm{d}z \tag{7}$$

In equation (7), the integral is calculated from 0 to infinity even though the size of the grain is finite. However, this is justified by the fact that the size of the depletion zone is much smaller than the size of the grain because the local concentration of Cr rapidly approaches the original concentration (C_{Cr}^0) at a sufficiently large distance from the depletion zone. By substituting equations (4) and (5) into equation (7), the following can be obtained

$$\Delta n_{Cr}^{\gamma} = \frac{S(x_{Cr}^0 - x_{Cr}^{\gamma\beta})}{V_m^{\gamma}}\int_0^{\infty}\mathrm{erfc}\left[\frac{z}{2(D_{Cr}t)^{1/2}}\right]\mathrm{d}z \tag{8}$$

Considering that the definite integral of the complementary error function erf$c$ is

$$\int_0^{\infty}\mathrm{erfc}(q)dq = \frac{1}{(\pi)^{1/2}} \tag{9}$$

equation (8) becomes

$$\Delta n_{Cr}^{\gamma} = \frac{S(x_{Cr}^0 - x_{Cr}^{\gamma\beta})}{V_m^{\gamma}}\frac{2(D_{Cr}t)^{1/2}}{(\pi)^{1/2}} \tag{10}$$

The mass balance of Cr requires that

$$\Delta n_{Cr}^{\beta} = \Delta n_{Cr}^{\gamma} \tag{11}$$

By substituting equations (6) and (10) into equation (11) and utilising equation (4), a condition for the quantity $\bar{r}$ is obtained

$$\bar{r} = \frac{V_m^{\beta}}{V_m^{\gamma}}\frac{\left(x_{Cr}^0 - x_{Cr}^{\gamma\beta}\right)}{\left(x_{Cr}^{\beta} - x_{Cr}^0\right)}\frac{2(D_{Cr}t)^{1/2}}{(\pi)^{1/2}} \tag{12}$$

The accumulation of carbon in the carbide phase is given by an equation analogous to equation (6)

$$\Delta n_C^{\beta} = (C_C^{\beta} - C_C^0)S\bar{r} \tag{13}$$

where C_C^{β} and C_C^0 are the concentrations of carbon in the carbide phase and in the original alloy respectively (cf. Fig. 1, lower diagram). The quantity C_C^{β} (and hence, x_C^{β}) results directly from the assumed stoichiometry of the carbide. The total depletion of C in the grain can be calculated as

$$\Delta n_C^{\gamma} = (C_C^0 - \overline{C_C^{\gamma}})Sd \tag{14}$$

where $\overline{C_C^{\gamma}}$ is the average concentration of carbon in the grain and d is the average distance over which carbon

can be withdrawn. In equation (14), the average concentration $\overline{C_C^{\gamma}}$ is used instead of integrating the carbon concentration C_C^{γ} throughout the grain. This approximation introduces a negligible error because the concentration of carbon shows a certain gradient only in the vicinity of the grain boundary (cf. Fig. 1), due to the change in the activity coefficient of carbon with the change in the concentration of substitutional elements. However, the size of the depletion zone is substantially smaller than the size of the grain. Hence, the distance over which the carbon concentration changes is much smaller than the distance over which it is effectively constant. Thus, the average concentration $\overline{C_C^{\gamma}}$ is essentially equivalent to the concentration of carbon at sufficiently large distances from the grain boundary, at which the gradients of concentrations become effectively zero.

The mass balance for carbon requires that

$$\Delta n_C^{\beta} = \Delta n_C^{\gamma} \tag{15}$$

Substituting equations (13) and (14) into equation (15) and utilising the expression for $\bar{r}$ given by equation (12), the authors obtain an expression for the carbon mole fraction in the grain

$$\overline{x_C^{\gamma}} = x_C^0 - \frac{2(D_{Cr}t)^{1/2}}{d(\pi)^{1/2}} \frac{x_C^{\beta} - x_C^0}{x_{Cr}^{\beta} - x_{Cr}^0} \left(x_{Cr}^0 - x_{Cr}^{\gamma\beta} \right) \tag{16}$$

Equation (16) is not an explicit expression for $\overline{x_C^{\gamma}}$ because the interfacial chromium concentration $x_{Cr}^{\gamma\beta}$ on the right-hand side of equation (16) depends on the carbon concentration $x_C^{\gamma\beta}$ through the paraequilibrium at the γ/β interface. The paraequilibrium condition for the reaction of carbide formation (equation 1) takes the form

$$K = \frac{1}{(a_{Cr}^{\gamma\beta})^{\nu_{Cr}} (a_C^{\gamma\beta})^{\nu_C}} \tag{17}$$

where K is the equilibrium constant, and the activities of Cr and C at the interface are denoted by $a_{Cr}^{\gamma\beta}$ and $a_C^{\gamma\beta}$ respectively. In equation (17), the activity of the carbide is equal to 1 because the carbide forms a separate phase. Equation (17) can be written in a more convenient form by relating the equilibrium constant K to the Gibbs energy of formation ΔG_f, i.e.

$$\Delta G_f^0 = -RT \ln K \tag{18}$$

which can be expressed as a function of temperature as

$$\Delta G_f^0 = A + BT \tag{19}$$

Equation (19) embodies the reasonable assumption that the enthalpy and entropy of formation are independent of temperature and is used to represent experimental Gibbs energy of formation data.[35] Rearrangement of equations (17) and (18) gives an expression for the activity of Cr at the grain boundary

$$\ln a_{Cr}^{\gamma\beta} = \frac{1}{\nu_{Cr}} \left(\frac{\Delta G_f^0}{RT} - \nu_C \ln a_C^{\gamma\beta} \right) \tag{20}$$

Equation (20) can be further rewritten by decomposing the activity into mole fractions and activity coefficients, i.e.

$$\ln x_{Cr}^{\gamma\beta} \gamma_{Cr}^{\gamma\beta}(\mathbf{x}^{\gamma\beta}, T) = \frac{1}{\nu_{Cr}} \left(\frac{\Delta G_f^0}{RT} - \nu_C \ln x_C^{\gamma\beta} \gamma_C^{\gamma\beta}(\mathbf{x}^{\gamma\beta}, T) \right) \tag{21}$$

where the activity coefficients are functions of the vector of composition $\mathbf{x}$ and temperature T. In addition to the thermodynamic equilibrium condition (21), the equality of carbon activities at the grain boundary and outside of the depletion zone (i.e. $a_C^{\gamma\beta} = \overline{a_C^{\gamma}}$) provides another condition.

$$x_C^{\gamma\beta} \gamma_C^{\gamma\beta}(\mathbf{x}^{\gamma\beta}, T) = \overline{x_C^{\gamma}}\, \overline{\gamma_C^{\gamma}}(\mathbf{x}^{\gamma}, T) \tag{22}$$

To apply equations (21) and (22), it is necessary to calculate the activity coefficients in the Cr–Ni–Fe–C system as a function of $\mathbf{x}$ and T. For this purpose, the authors use the activity coefficient formulation developed by Babu *et al.*[36] for Fe–Ni–Cr–Mo–C–N alloys on the basis of the models of Hertzman,[37,38] Hertzman and Jarl[39] and Andersson and Lange.[40] Conditions (21) and (22) are supplemented by the normalisation condition for mole fractions

$$\sum_i x_i^{\gamma\beta} = 1 \tag{23}$$

and the requirement that the molar ratio of the alloy components that do not participate in carbide formation be constant in the grain[10]

$$\frac{x_{Fe}^{\gamma\beta}}{x_{Ni}^{\gamma\beta}} = \frac{x_{Fe}^0}{x_{Ni}^0} \tag{24}$$

Equations (16) and (21)–(24) constitute a set of five equations, which can be solved numerically with respect to the four mole fractions at the interface $x_i^{\gamma\beta}$ (i=Cr, Ni, Fe, C) and the mole fraction of carbon in the matrix outside of the depletion zone $\overline{x_C^{\gamma}}$. The remaining mole fractions in the matrix outside of the depletion zone (i.e. x_i^{γ} for i=Cr, Ni, Fe) are essentially the same as those in the original alloy (x_i^0) except for a slight renormalisation to accommodate the changes in the matrix carbon concentration $\overline{x_C^{\gamma}}$ in each iteration. In a practical implementation, the two linear constraints (equations (23) and (24)) are used to eliminate two variables $x_{Fe}^{\gamma\beta}$ and $x_{Ni}^{\gamma\beta}$, which leaves three non-linear equations (equations (16), (21) and (22)) to be solved numerically. For optimum numerical stability, Equations (21) and (22) are then solved with respect to $x_{Cr}^{\gamma\beta}$ and $x_C^{\gamma\beta}$ for a given value of $\overline{x_C^{\gamma}}$ in an inner loop, and equation (16) is converged with respect to $\overline{x_C^{\gamma}}$ in an outer loop.

Once the value of $x_{Cr}^{\gamma\beta}$ is found for a given temperature and time of exposure, the Cr concentration profile $x_{Cr}^{\gamma}(z,t)$ is calculated from equation (5) as a function of the distance z from the grain boundary and time. The corresponding concentration profiles of the other elements are then found from equations that are analogous to equations (23)–(24) but in which the local concentrations in the matrix $x_i^{\gamma}(z,t)$ (i=Ni, Fe) are substituted instead of the grain boundary concentrations $x_i^{\gamma\beta}$.

It should be noted that the thermodynamic model of carbide formation implies that the minimum chromium concentration is achieved at the very beginning of the heat exposure (t=0) because carbon concentration is

then at its highest value. It is known, however, that the time to reach the minimum Cr concentration is finite rather than zero. Various approaches to account for this observation have been proposed in the literature.[13,29–31] Here, the authors adopt the approach of Sourmail *et al.*,[30] who explained the delay in reaching the minimum of Cr depletion by considering the average composition that is measured rather than the exact predicted interface composition. Sourmail *et al.*[30] argued that the measurements are likely to overestimate the actual interface composition because of strong concentration gradients in the vicinity of the grain boundary, which cause the measured values to reflect an averaged effect due to beam spreading. Because of this effect, coupled with the problems of relative orientation of the grain boundary and the beam, Sourmail *et al.*[30] proposed to calculate the measurable concentration as the average over a finite range in a direction perpendicular to the boundary. At distances z close to the boundary, such an averaged value is significantly different from the local value when the concentration gradient is steep. As the authors move farther from the boundary, the average value rapidly approaches the local value. Thus, the averaged, measurable concentration at a distance z from the grain boundary is calculated as

$$\overline{x_i^{\gamma}}(z) = \frac{1}{\Delta z}\int_{z-\Delta z/2}^{z+\Delta z/2} x(z)\mathrm{d}z \tag{25}$$

where Δz is assumed to be 20 nm. The averaged value can be then compared with the results of experimental measurements. At distances close to the grain boundary, the averaged concentration naturally decreases as a function of time in a relatively short time interval, then reaches a minimum and finally increases.

This approach to calculating the measurable local concentration is sufficient for the study of localised corrosion because the authors are not concerned here with the detailed calculation of time evolution in the initial stages of chromium depletion. The accurate prediction of depletion profiles over a larger interval of time is much more important.

As discussed above, the growth of the carbide strongly depends on the volume (i.e. $V=Sd$) from which carbon is withdrawn. If the available distance d is small, the carbon concentration rapidly drops to the solubility limit, and self-healing starts after a short amount of time. Conversely, if d is infinite, self-healing will never occur because the carbon concentration will remain at its bulk value. Following Sourmail *et al.*,[30] the authors assume that d is equal to one-sixth of the average size of the grain, i.e.

$$d = \frac{g}{6} \tag{26}$$

where g is the average grain size. Equation (6) was postulated[30] for the sensitisation of Fe–Ni–Cr–C alloys by arguing that, since soft-impingement is a three-dimensional phenomenon, it is appropriate to attribute to the calculation volume a sixth of the grain given that, if a cubic model is used to represent the grain, six faces will actually draw the carbon from the same volume.

In total, the chromium depletion model contains the following parameters:

(i) parameters A and B for calculating the Gibbs energy of formation of the carbide as a function of temperature (equation (19))

(ii) parameters D_{Cr}^0 and Q_{Cr} for calculating the diffusion coefficient of Cr as a function of temperature according to the general relation

$$D_i = D_i^0 \exp\frac{Q_i}{RT}\ (i=\mathrm{Cr}) \tag{27}$$

(iii) the average grain size g

In principle, all these parameters can be obtained from independent experimental data, but they may be adjusted in practice to match concentration profile data.

Extension of model to Mo depletion

Assuming that multicomponent diffusion effects can be neglected, the molybdenum concentration profile can be calculated from equations analogous to equations (2)–(5). The mole fraction of Mo as a function of time and distance from the grain boundary is then given by

$$x_{\mathrm{Mo}}^{\gamma}(z,t) = x_{\mathrm{Mo}}^{\gamma\beta} + (x_{\mathrm{Mo}}^0 - x_{\mathrm{Mo}}^{\gamma\beta})\mathrm{erf}\left[\frac{z}{2(D_{\mathrm{Mo}}t)^{1/2}}\right] \tag{28}$$

The accumulation of Mo in the carbide phase can be obtained from an equation analogous to equation (6)

$$\Delta n_{\mathrm{Mo}}^{\beta} = (C_{\mathrm{Mo}}^{\beta} - C_{\mathrm{Mo}}^0)S\bar{r} \tag{29}$$

As with Cr, the total depletion of Mo in the grain can be calculated by integrating the local depletion over the entire grain by using equations analogous to equations (7–10). This yields

$$\Delta n_{\mathrm{Mo}}^{\gamma} = \frac{S\left(x_{\mathrm{Mo}}^0 - x_{\mathrm{Mo}}^{\gamma\beta}\right)}{V_{\mathrm{m}}^{\gamma}}\frac{2(D_{\mathrm{Mo}}t)^{1/2}}{(\pi)^{1/2}} \tag{30}$$

Using the mass balance constraint for Mo, i.e.

$$\Delta n_{\mathrm{Mo}}^{\beta} = \Delta n_{\mathrm{Mo}}^{\gamma} \tag{31}$$

an equation for the average dimension of the carbide along the z axis can be obtained

$$\bar{r} = \frac{V_{\mathrm{m}}^{\beta}\left(x_{\mathrm{Mo}}^0 - x_{\mathrm{Mo}}^{\gamma\beta}\right)}{V_{\mathrm{m}}^{\gamma}\left(x_{\mathrm{Mo}}^{\beta} - x_{\mathrm{Mo}}^0\right)}\frac{2(D_{\mathrm{Mo}}t)^{1/2}}{(\pi)^{1/2}} \tag{32}$$

Since the quantity $\bar{r}$ obtained from equation (32) must be the same as that obtained from equation (12), a relationship between the mole fractions of Mo and Cr at the γ/β boundary is obtained

$$x_{\mathrm{Mo}}^{\gamma\beta} = x_{\mathrm{Mo}}^0 - \left(x_{\mathrm{Cr}}^0 - x_{\mathrm{Cr}}^{\gamma\beta}\right)\frac{x_{\mathrm{Mo}}^{\beta} - x_{\mathrm{Mo}}^0}{x_{\mathrm{Cr}}^{\beta} - x_{\mathrm{Cr}}^0}\left(\frac{D_{\mathrm{Cr}}}{D_{\mathrm{Mo}}}\right)^{1/2} \tag{33}$$

To apply equation (33), it is necessary to know the mole fractions in the carbide phase, x_{Mo}^{β} and x_{Cr}^{β}. For this purpose, the authors assume the overall metal carbide stoichiometry $M_{v_{\mathrm{M}}}C_{v_{\mathrm{C}}}$, where the typical values of v_{M} and v_{C} are 23 and 6 or 7 and 3 respectively. Then, the following equation can be written

$$\frac{x_{\mathrm{Cr}}^{\beta} + x_{\mathrm{Mo}}^{\beta}}{x_{\mathrm{C}}^{\beta}} = \frac{v_{\mathrm{M}}}{v_{\mathrm{C}}} \tag{34}$$

In addition, it is necessary to specify the ratio of the mole fractions of Mo and Cr in the carbide phase, i.e.

$$\frac{x_{\mathrm{Mo}}^{\beta}}{x_{\mathrm{Cr}}^{\beta}} = m \tag{35}$$

In principle, this value can be obtained from experimental measurements. In some cases (e.g. in alloy 825),[14] this ratio does not differ much, on average, from the molar ratio of Mo to Cr in the bulk alloy. In the absence of experimental data, the ratio m can be assumed to be equal to that in the bulk alloy as a default value. From equations (34) and (35), the mole fractions in the carbide phase can be calculated as

$$x_{\mathrm{Mo}}^{\beta} = \frac{m(\nu_{\mathrm{M}}/\nu_{\mathrm{C}})}{(1+m)(1+\nu_{\mathrm{M}}/\nu_{\mathrm{C}})} \tag{36}$$

$$x_{\mathrm{Cr}}^{\beta} = \frac{\nu_{\mathrm{M}}/\nu_{\mathrm{C}}}{(1+m)(1+\nu_{\mathrm{M}}/\nu_{\mathrm{C}})} \tag{37}$$

In the next step, it is necessary to generalise the thermodynamic paraequilibrium relationships for carbide formation (equations (1) and (17)–(21)). Reaction (1) can be generalised for a mixed carbide

$$\nu_{\mathrm{Cr}}\mathrm{Cr} + \nu_{\mathrm{Mo}}\mathrm{Mo} + \nu_{\mathrm{C}}\mathrm{C} = \mathrm{Cr}_{\nu_{\mathrm{Cr}}}\mathrm{Mo}_{\nu_{\mathrm{Mo}}}\mathrm{C}_{\nu_{\mathrm{C}}} \tag{38}$$

The formation reaction (equation (38)) can be formally separated using two thermodynamically equivalent forms

$$\frac{\nu_{\mathrm{Cr}}}{\nu_{\mathrm{M}}}(\nu_{\mathrm{M}}\mathrm{Cr} + \nu_{\mathrm{C}}\mathrm{C}) + \frac{\nu_{\mathrm{Mo}}}{\nu_{\mathrm{M}}}(\nu_{\mathrm{M}}\mathrm{Mo} + \nu_{\mathrm{C}}\mathrm{C}) = \mathrm{Cr}_{\nu_{\mathrm{Cr}}}\mathrm{Mo}_{\nu_{\mathrm{Mo}}}\mathrm{C}_{\nu_{\mathrm{C}}} \tag{39}$$

and

$$\frac{\nu_{\mathrm{Cr}}}{\nu_{\mathrm{M}}}\mathrm{Cr}_{\nu_{\mathrm{M}}}C_{\nu_{\mathrm{C}}} + \frac{\nu_{\mathrm{Mo}}}{\nu_{\mathrm{M}}}\mathrm{Mo}_{\nu_{\mathrm{M}}}\mathrm{C}_{\nu_{\mathrm{C}}} = \mathrm{Cr}_{\nu_{\mathrm{Cr}}}\mathrm{Mo}_{\nu_{\mathrm{Mo}}}\mathrm{C}_{\nu_{\mathrm{C}}} \tag{40}$$

Hence, it is convenient to decompose equation (38) into two reactions

$$\nu_{\mathrm{M}}\mathrm{Cr} + \nu_{\mathrm{C}}\mathrm{C} = \mathrm{Cr}_{\nu_{\mathrm{M}}}\mathrm{C}_{\nu_{\mathrm{C}}} \tag{41}$$

$$\nu_{\mathrm{M}}\mathrm{Mo} + \nu_{\mathrm{C}}\mathrm{C} = \mathrm{Mo}_{\nu_{\mathrm{M}}}\mathrm{C}_{\nu_{\mathrm{C}}} \tag{42}$$

Following equations (17–20), it is easy to show that the thermodynamic relations for equations (41) and (42) are

$$\ln a_{\mathrm{Cr}}^{\gamma\beta} = \frac{1}{\nu_{\mathrm{M}}}\left[\frac{\Delta G_{\mathrm{f}}^{0}(\mathrm{Cr}_{\nu_{\mathrm{M}}}\mathrm{C}_{\nu_{\mathrm{C}}})}{\mathrm{RT}} - \nu_{\mathrm{C}}\ln a_{\mathrm{C}}^{\gamma\beta}\right] \tag{43}$$

$$\ln a_{\mathrm{Mo}}^{\gamma\beta} = \frac{1}{\nu_{\mathrm{M}}}\left[\frac{\Delta G_{\mathrm{f}}^{0}(\mathrm{Mo}_{\nu_{\mathrm{M}}}\mathrm{C}_{\nu_{\mathrm{C}}})}{RT} - \nu_{\mathrm{C}}\ln a_{\mathrm{C}}^{\gamma\beta}\right] \tag{44}$$

The main advantage of this decomposition is the fact that equation (43) is algebraically equivalent to equation (20) or (21). Equations (16) and (22)–(24) remain unchanged for systems containing Mo. Thus, the system is described by seven equations, i.e. equations (16), (22)–(24), (33), (43) and (44), which can be solved with respect to the five mole fractions at the interface $x_{\mathrm{i}}^{\gamma\beta}$ (i=Cr, Mo, Ni, Fe, C) and the mole fraction of carbon in the matrix outside of the depletion zone $\overline{x_{\mathrm{C}}^{\gamma}}$. Since one of the equations is redundant, it is convenient to use equation (33) and eliminate equation (44) because equation (33) provides a straightforward linear constraint, and the additional thermodynamic parameter $\Delta G_{\mathrm{f}}^{0}(\mathrm{Mo}_{\nu_{\mathrm{M}}}\mathrm{C}_{\nu_{\mathrm{C}}})$ does not need to be known then. After solving equations (16), (22)–(24), (33) and (43), equation (44) may be used for testing the consistency of the solution as long as $\Delta G_{\mathrm{f}}^{0}(\mathrm{Mo}_{\nu_{\mathrm{M}}}\mathrm{C}_{\nu_{\mathrm{C}}})$ can be estimated with sufficient accuracy.

Using this approach, calculation of depletion profiles for molybdenum-containing systems requires two additional parameters in addition to those used for computing the Cr depletion profiles as described above, i.e.

(iv) the diffusion coefficient of Mo, which is calculated from the standard equation (27) where i=Mo
(v) the Mo/Cr molar ratio in the carbide (equation (35)), which can be obtained from experimental data or adjusted based on Mo depletion profiles.

Effective size of depletion zone

The effective size of the depletion zone provides information on the width of the depletion zone in a direction perpendicular to the grain boundary. The depletion profile does not automatically define the size of the depletion zone because it asymptotically approaches the bulk concentration of Cr (cf. Fig. 1, upper diagram). Therefore, to evaluate the effective size of the depletion zone z_{eff}, the authors can approximate the chromium depletion zone by a triangle with the vertices defined by C_{Cr}^{0} and $C_{\mathrm{Cr}}^{\gamma\beta}$ along the concentration axis (cf. Fig. 1) and z_{eff} along the z axis. Then, the total depletion of chromium $\Delta n_{\mathrm{Cr}}^{\gamma}$, calculated from the triangular approximation, should be equal to that obtained by rigorous integration from zero to infinity (equation 10). From simple geometrical considerations, the total depletion calculated using the approximate triangle is equal to

$$\Delta n_{\mathrm{Cr}}^{\gamma} = S(C_{\mathrm{Cr}}^{0} - C_{\mathrm{Cr}}^{\gamma\beta})\frac{z_{\mathrm{eff}}}{2} = \frac{1}{2}\frac{S}{V_{\mathrm{m}}^{\beta}}(x_{\mathrm{Cr}}^{0} - x_{\mathrm{Cr}}^{\gamma\beta})z_{\mathrm{eff}} \tag{45}$$

By equating $\Delta n_{\mathrm{Cr}}^{\gamma}$ calculated from equations (10) and (45), the following equation can be obtained

$$z_{\mathrm{eff}} = \frac{4(D_{\mathrm{Cr}}t)^{1/2}}{(\pi)^{1/2}} \tag{46}$$

Repassivation potential model

In a previous paper,[19] a comprehensive model was developed to calculate the repassivation potential of bulk alloys as a function of environment chemistry and temperature. Since the details of this model were described previously,[19,24] only its essential features are summarised here. The model was derived by considering the dissolution of a metal in a localised corrosion environment in the limit of repassivation. The model envisages the dissolution of the metal (M) underneath a layer of a concentrated metal halide solution MX. In the process of repassivation, a thin layer of oxide is assumed to form at the interface between the metal and the hydrous metal halide. The model represents the formation of the oxide layer using a partial coverage approach. The partial coverage fraction increases as repassivation is approached. The dissolution rate of the metal under the oxide is lower than at the metal/halide interface and corresponds to the passive dissolution rate. Thus, as the repassivation potential is approached, the dissolution rate tends towards the passive dissolution

rate. The model includes the effects of multiple aggressive and non-aggressive or inhibitive species, which are assumed to undergo competitive adsorption. The aggressive species form metal complexes, which dissolve in the active state. The inhibitive species and water contribute to the formation of oxides, which induce passivity. The formalism that describes these phenomena leads to a closed-form equation in the limit of repassivation, i.e. when the current density reaches a predetermined low value i_{rp} (assumed to be $i_{rp}=10^{-2}$ A m^{-2}) and the fluxes of metal ions become small and comparable to those for passive dissolution. Most importantly, for the study of thermally aged alloys, the parameters of the model have been generalised in terms of alloy composition for Fe–Ni–Cr–Mo–W–N alloys.[24] This generalisation was based on experimental E_{rp} data for 13 base (typically mill-annealed) stainless steels and nickel-based alloys, supplemented by those for Fe and Ni. The Appendix summarises the final working equations for the E_{rp} model, defines the model parameters and provides the equations for calculating the parameters as functions of alloy composition. Thus, Appendix contains a complete recipe for predicting the repassivation potential as a function of alloy composition, aqueous environment temperature and chloride activity. This model will be used further in this study to predict the repassivation potentials of heat-treated alloys.

Effective repassivation potential of sensitised alloys

The two models described above (i.e. the local Cr/Mo depletion model and the E_{rp} model) make it possible to calculate the hypothetical 'local' repassivation potential at each microscopic point on the alloy surface. However, a question arises as to how the macroscopically measured repassivation potential is related to local microchemistry. Specifically, does the localised corrosion sense the minimum in the depletion profile or some kind of average? A somewhat similar problem has been investigated for sensitised alloys in environments that cause uniform, passive corrosion except in the presence of grain boundary depletion.[41,42] Such phenomena can be investigated using electrochemical potentiodynamic reactivation (EPR) tests. In particular, Gaudett and Scully[41] examined the distribution of grain boundary Cr depletion and its effect on the degree of sensitisation as measured by EPR tests. They found that IGSCC failure occurs when the boundary Cr concentration is depleted to below a certain critical level, and also, more than a certain fraction of grain boundaries must be depleted to the critical level to observe macroscopic IGSCC. Jiang *et al.*[42] also examined the effect of Cr-rich and depleted zones in duplex stainless steels due to the α' phase in sulphuric acid using the EPR technique. They established a correlation between reactivation kinetics and the percentage of atomic layers that have Cr less than a certain value and developed an averaging scheme that predicts the active dissolution current of the ferrite by averaging over the local zones. However, these literature sources[41,42] focus on the active–passive dissolution regime and do not discuss the core topic of this study, i.e. the crevice/pitting corrosion that may occur even in the absence of grain boundary alloying element depletion, but can be accelerated by the depletion. In intergranular corrosion or EPR tests, the size of the corrosion defect does not need to be considered. However, in the present study, the effect of depletion zone size in comparison to the size of the pits is crucial because, unlike in intergranular corrosion or IGSCC,[41,42] pitting requires a critical size to stabilise the pit chemistry. Without exceeding this critical size, pits/crevices will not be stable. This major difference requires developing an approach that takes into account the size of the area that is subject to localised corrosion.

A previous study[18] has demonstrated that the dependence of the repassivation potential on heat treatment time does not correlate with that of the degree of sensitisation (as determined by EPR). This observation has provided an indication that, unlike the degree of sensitisation, the repassivation potential of sensitised samples is not merely a reflection of Cr depletion below a certain threshold level.[18] In contrast to intergranular dissolution, which occurs primarily in the Cr-depleted regions, pitting/crevice corrosion can occur in both Cr-depleted and non-depleted areas. Further, the rate of dissolution inside a pit or active crevice region is not likely to be dramatically different between a Cr-depleted and non-depleted material because localised corrosion occurs in a completely active state in a highly aggressive environment. In repassivation potential tests, the potential at which the rate of oxide film formation exceeds the active dissolution rate is measured as a function of heat treatment. This process is expected to be different between the Cr-depleted and non-depleted areas, leading to a different potential at which the oxide film is stabilised as a function of local alloy composition.

The repassivation potential model described above can be directly used to predict local values of E_{rp} on the basis of the local Cr (and Mo) concentration as a function of the distance from the grain boundary. However, such local values of E_{rp} are not experimentally accessible. This is due to the fact that the measured repassivation potential is a macroscopic property, i.e. it reflects the repassivation of several pits with dimensions ranging from several hundred micrometres to a millimetre. These dimensions are much larger than the depletion zone sizes, and therefore, each pit can be imagined to contain several depleted grain boundaries at the bottom of the pit. In principle, it would be possible to calculate the averaged repassivation potential if the geometry of the pit was exactly known and the composition of the alloy that is exposed to the pit environment could be exactly ascertained. However, information about the pit geometry and alloy composition at the bottom of the pit is not available in practice and even if it were available, prediction of E_{rp} based on detailed measurements of individual pits would be of little predictive value for corroding structures. Instead, it is necessary to establish a procedure for estimating the average repassivation potential for statistically distributed pits. Such a procedure is made possible by the fact that plentiful experimental information is available about the dependence of the repassivation potential on the composition of bulk Fe–Ni–Cr–Mo–W–N alloys.[24] Furthermore, this information is embodied in a computational model. To calculate E_{rp} of thermally aged samples, it is reasonable to make the following assumptions:

(i) the measured E_{rp} primarily reflects the localised corrosion of the Cr-depleted regions rather than

of the surfaces whose Cr concentration is given by the nominal alloy composition. This is due to the fact that a pit stabilises more easily in an area that is more susceptible to localised corrosion because of chromium (or molybdenum) depletion. The experimentally observed localised corrosion occurred predominantly in the grain boundary area.[18] Even if some localised corrosion occurs outside of the depleted zones, the repassivation potential calculated over the depletion zone should provide a conservative (i.e. lower) estimate, which is desirable in engineering practice. Thus, the average repassivation potential should be calculated by integrating the E_{rp} over the depleted zone

(ii) a pit needs to achieve a certain minimum size to be stabilised in an E_{rp} measurement. Therefore, in the case of a narrow Cr depletion zones, the averaging should extend beyond the depletion zone to ensure that a certain minimum area of the alloy contributes to the measurable E_{rp}.

Following assumption (i), the average repassivation potential $\overline{E_{rp}}$ can be obtained by integration of the local repassivation potential, $E_{rp}(z)$, as follows

$$\overline{E_{rp}} = \frac{\int_0^L w(z)E_{rp}(z)dz}{\int_0^L w(z)dz} \tag{47}$$

where L is the distance from the grain boundary over which the integration is performed and $w(z)$ is a weighting factor, which reflects, in principle, the uneven contribution of the depleted zone surface to the observable repassivation potential. In view of assumption (i), the distance for integration L can be identified with the effective size of the depletion zone z_{eff} (equation (46)). However, this value should be adjusted in agreement with assumption (ii) to ensure that the repassivation potential is integrated over at least a certain reasonable minimum distance from the grain boundary. Thus, the distance for integration can be estimated as

$$L = z_{eff} + 2\Delta z \tag{48}$$

where z_{eff} is calculated from equation (46), and $2\Delta z$ is the minimum size for stabilisation of localised corrosion. For simplicity, Δz is set at the same value as that used to calculate the observable depletion profiles (equation (25)). The expression for z_{eff} obtained from equation (46) is somewhat arbitrary because a different value could be obtained, for example, on the basis of the molybdenum depletion profile. However, the precise definition of the effective size is not crucial for integrating the repassivation potential over the depletion zone. With equation (48), the repassivation potential is effectively integrated over the depletion zone when the zone is reasonably wide. When it is very narrow, the integration is effectively performed over the minimum distance.

The weighting factor $w(z)$ for the integration should recognise that the contribution of the depleted areas with Cr concentration below a threshold value (e.g. $x^*_{Cr} = 0{\cdot}12$) should be greater than the contribution of the areas in which Cr is less severely depleted. For this purpose, the authors define $w(z)$ as follows

$$w(z) = 1 + \eta \max\left(\frac{x^*_{Cr} - x_{Cr}(z)}{x^*_{Cr}}, 0\right) \tag{49}$$

In equation (49), the term in parentheses ensures that the weighting factor is equal to 1 for all chromium concentrations above the threshold value (i.e. when $x_{Cr}(z) \geqslant x^*_{Cr}$) and becomes progressively enhanced as the Cr concentration drops below x^*_{Cr}. The enhancement factor η is assumed to be equal to 100, which is the order of magnitude of the elevation of dissolution rates in Cr-depleted areas in standard tests in acidic solutions. While equation (49) is arbitrary, it provides a reasonable enhancement of the weighting factor for the Cr compositions that fall below x^*_{Cr}. The minimum value of $w(z)$ is 1, while the maximum value is $1+\eta$. Thus, the averaged repassivation potential for heat-treated samples can be obtained from equations (47)–(49), where the local value of the repassivation potential $E_{rp}(z)$ is calculated from the generalised repassivation potential model (as described in Appendix) using the local alloy compositions obtained from the Cr and Mo depletion profiles as a function of the distance from the grain boundary.

This method of averaging can be compared with the computation of E_{rp} directly at the grain boundary, where the Cr concentration is at its minimum and therefore, the repassivation potential reaches its lowest value. It can be expected that the method of averaging should give reasonable predictions if a critical size needs to be accounted for as discussed above. On the other hand, the E_{rp} value calculated at the grain boundary will reflect a different hypothetical scenario, in which, in the process of repassivation, most of the surface is already repassivated and the only remaining activity is in little grooves at the grain boundaries. In such a situation, the measured E_{rp} value should correspond to the local boundary concentration of Cr/Mo. These two scenarios will be tested against experimental data below.

Results

In this section, the authors first verify the grain boundary microchemistry model by comparing the calculated depletion profiles with experimental data. Then, the authors calculate the repassivation potentials of thermally aged and welded alloys using the procedures described above.

Depletion profiles

The grain boundary microchemistry model has been verified using experimental data for alloys 600, 825 and 316L. The model parameters for these alloys and the sources of experimental data are summarised in Table 2. The parameters A and B were determined by regressing depletion data simultaneously for various samples of a given alloy. As shown in Table 2, the only sample-specific parameter is the average grain size, and the remaining parameters are general for a given alloy. However, the predicted depletion profiles are rather less sensitive to the grain size than to the remaining parameters, and the effect of grain size manifests itself only at relatively advanced stages of healing because the grain size determines the available supply of carbon. In addition, Table 2 gives the average deviations between the calculated and experimental concentrations of Cr and Mo.

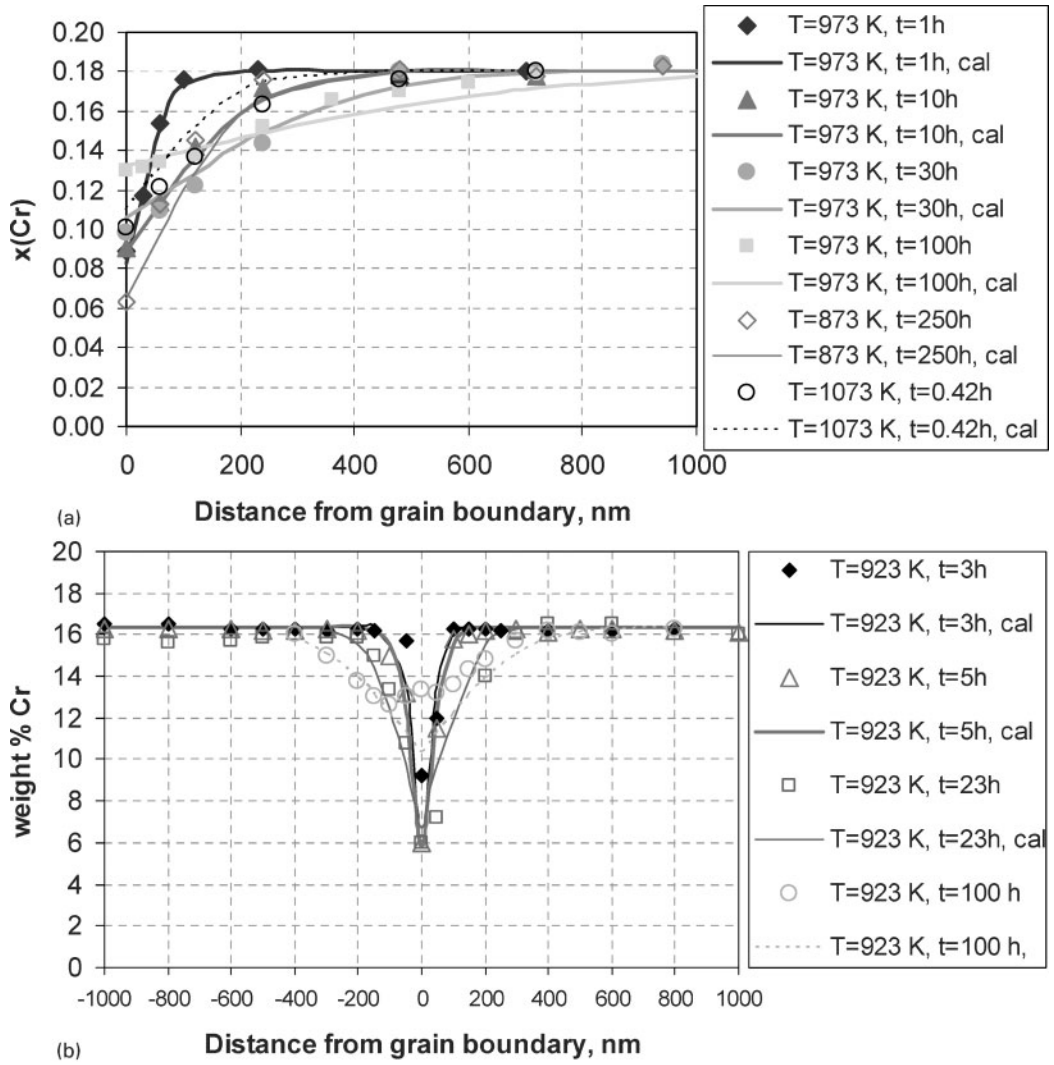

2 Calculated and experimental chromium depletion profiles of heat-treated alloy 600 for various aging temperatures and times. Experimental data are from Was and Kruger[10] *a* and Hall and Briant[8] *b*

In the case of alloy 600, experimental data are available from three sources.[8,10,43] These three data sets are in reasonably good agreement with each other. Model calculations are compared with selected experimental data in Fig. 2. The two diagrams in Fig. 2 illustrate the progressive self-healing (i.e. the increase in the minimum Cr concentration and the concomitant widening of the depletion profiles) for sensitised samples aged at 973 K (Fig. 2*a*) and 923 K (Fig. 2*b*) as a function of aging time. For comparison, depletion profiles are also shown for lower aging temperature and longer aging time (873 K, 250 h) and higher temperature and shorter time (1073 K, 0·42 h) Good agreement has been obtained with all data sets, in particular with the data of Was and Kruger.[10]

For alloy 825, chromium depletion data are available from the study of Pan *et al.*[14] Figure 3 compares the calculated and experimental results for this alloy. The time evolution of the depletion profiles is shown for samples thermally aged at 913 K (Fig. 3*a*) and at temperatures ranging from 973 to 1073 K (Fig. 3*b*). Because of a higher Cr content of alloy 825 compared with that of alloy 600, the grain boundary Cr concentration does not drop to values as low as those observed in Fig. 2. The model calculations are in agreement with the data within the experimental scattering range. To calculate both Cr and Mo depletion profiles, it was assumed that the Mo/Cr ratio in the carbide is identical to that in the bulk alloy, which is consistent with the carbide composition results reported by Pan *et al.*[14] However, molybdenum depletion profiles are not available for this alloy so that a comparison cannot be made.

On the other hand, some experimental Mo depletion profiles are available for type 316L stainless steel. In this case, experimental Cr depletion data are particularly abundant as shown in Table 2. Selected results of calculations are shown for this alloy in Fig. 4. Figure 4*a* shows the time evolution of depletion profiles for a relatively low aging temperature (823 K) and long times. Figure 4*b* illustrates the Cr depletion profiles for a fixed aging time (1000 h) and temperatures varying from 873 to 1023 K. The widening of the profiles and the increase in the minimum Cr concentration as a function of aging temperature at constant aging time are correctly reproduced. Figure 4*c* shows the molybdenum depletion profile at the conditions that correspond to the Cr profiles in Fig. 4*a*. For type 316L stainless steel, the Mo/Cr ratio was adjusted to reproduce the depletion profiles and is listed in Table 2 together with the remaining

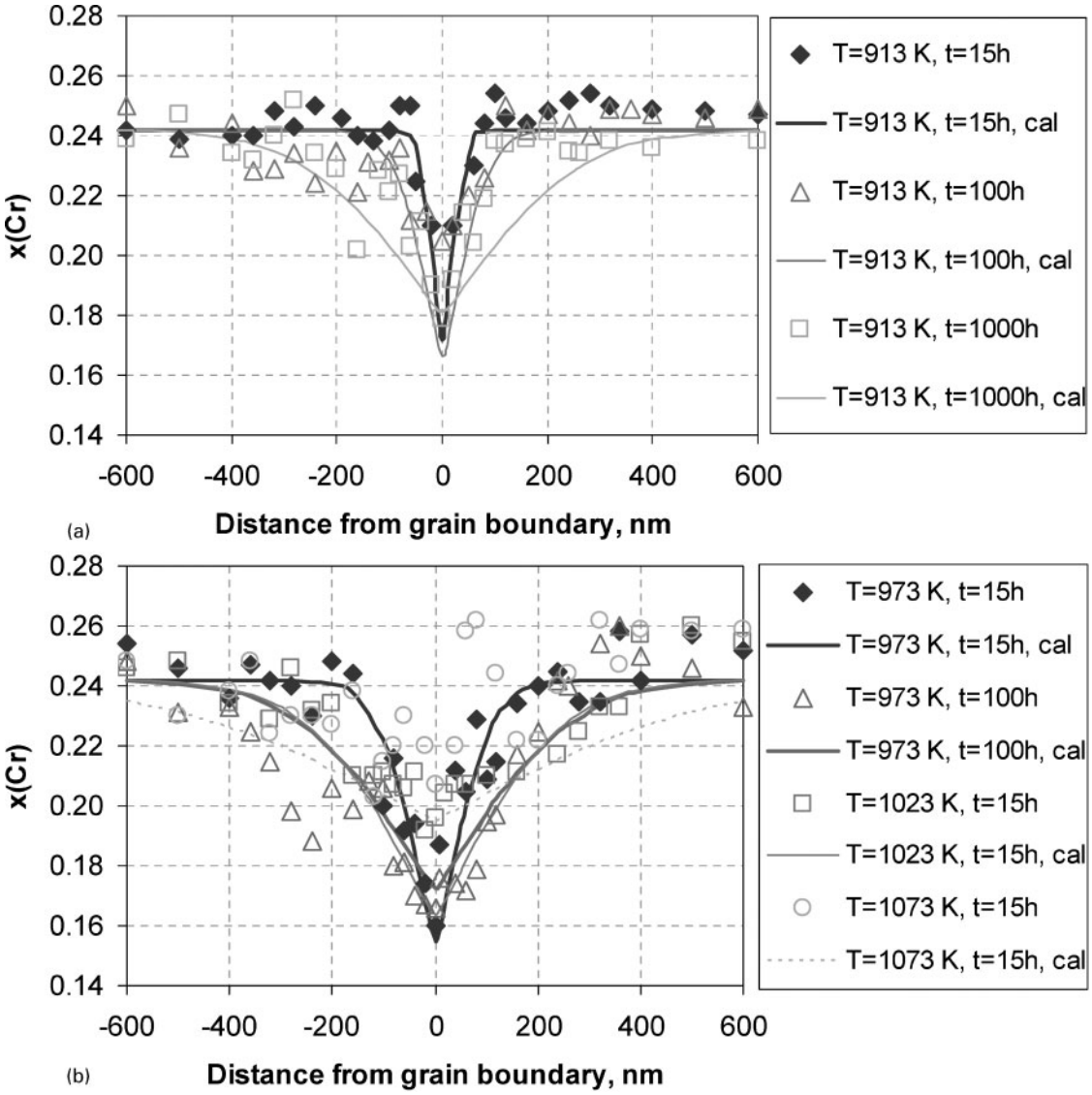

3 Calculated and experimental chromium depletion profiles for alloy 825 thermally aged at *a* 913 K and *b* 973–1073 K. Experimental data are from Pan *et al.*[14]

parameters. Thus, the model simultaneously reproduces the Cr and Mo depletion profiles generally within the uncertainty of experimental data.

Repassivation potential of thermally aged samples

Figures 5 and 6 show the results of modelling the repassivation potential for alloy 600. Figure 5 summarises the dependence of the repassivation potential of mill-annealed samples on temperature and the activity of chloride ions.[24] The lines in Fig. 5 have been obtained from the correlation described in Appendix. Over most of the chloride range, E_{rp} shows the standard semi-logarithmic dependence on chloride activity. This dependence provides a baseline for calculating E_{rp} of thermally aged samples.

Figure 6 shows the difference between the repassivation potentials of solution annealed and thermally aged samples and those of mill-annealed samples, i.e.

$$\Delta E_{rp} = E_{rp} - E_{rp,\text{mill-annealed}} \quad (50)$$

The experimental E_{rp} data have been reported in a previous paper[18] for samples aged at 700°C as a function of time. The repassivation potentials have been measured at 60°C in 0·001, 0·005 and 0·04M NaCl solutions. The measurements have been performed on alloy 600 with 0·02%C at all conditions and on samples with 0·04%C in 0·001 and 0·04M NaCl solutions.

The calculations have been performed using the averaging procedure described above and by assuming the alloy composition at the grain boundary. In Fig. 6, the thick lines show the averaged repassivation potentials predicted according to equations (48)–(50). The thin lines represent the minimum value of the repassivation potential, which corresponds to the minimum predicted concentration of chromium at the grain boundary. Additionally, the dotted line in the middle diagram in Fig. 6 (i.e. the one for 0·005M solutions) shows the results obtained using the averaging procedure without the weighting factor (equation (49)). The experimental data are plotted with error bars of ± 50 mV, which is a reasonable estimate for the uncertainty of E_{rp} measurements. Comparison between the calculated and experimental values reveals that the predictions obtained using the weighted averaging procedure agree, in general, with the data for the 0·02%C alloy within the experimental

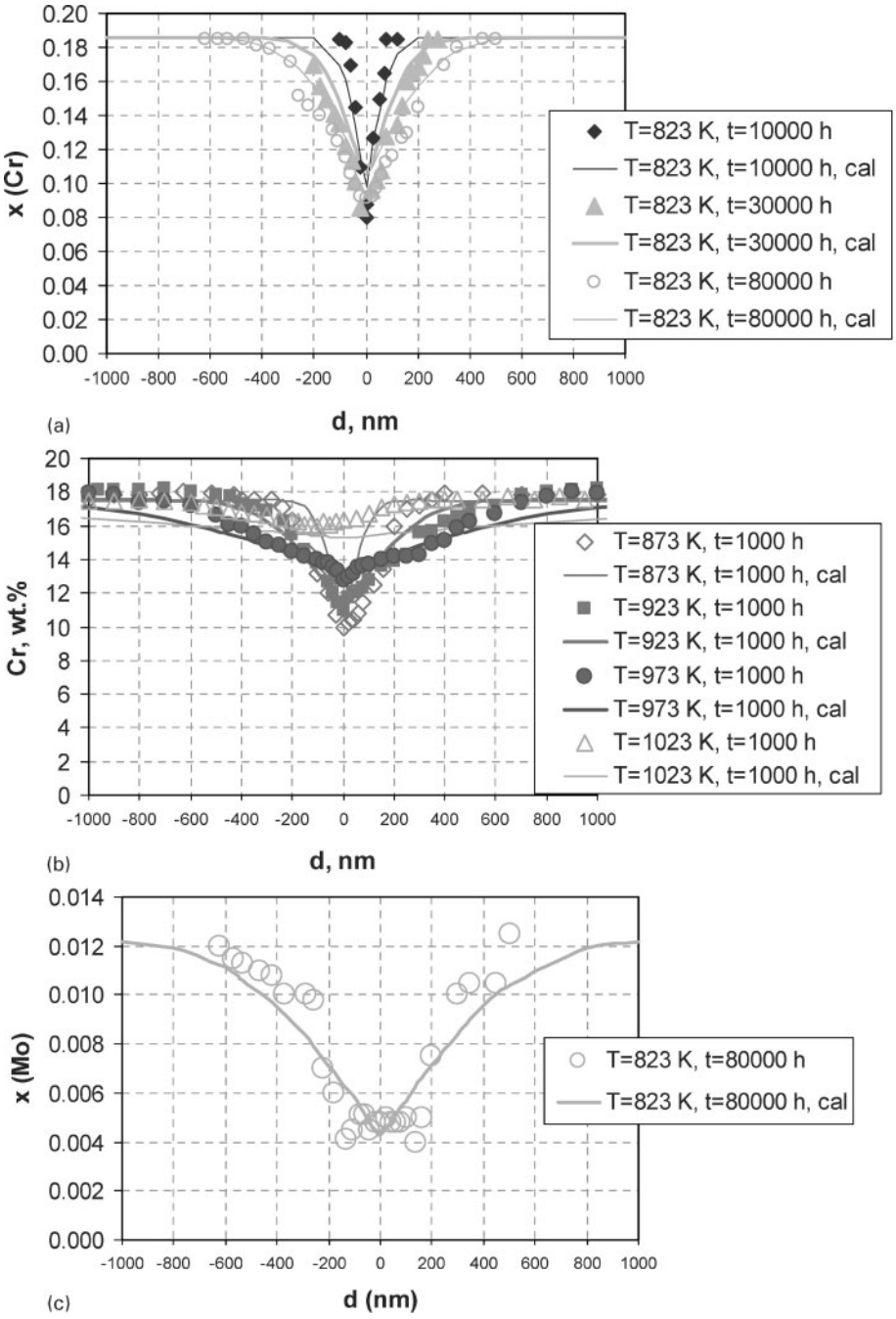

4 ***a*, *b*** **Calculated and experimental chromium and** ***c*** **molybdenum depletion profiles for heat-treated type 316 stainless steel. The data are from Sahlaoui *et al.*[44] (*a*, *c*) and Tekin *et al.*[45] (*b*)**

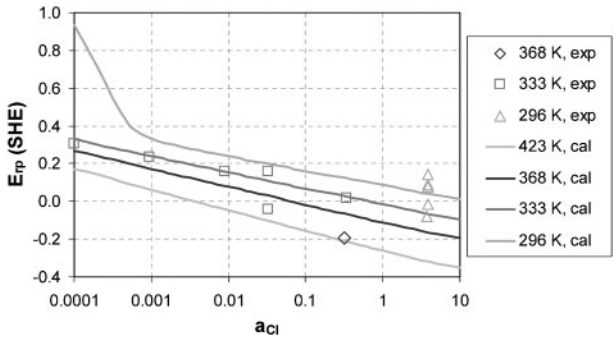

5 Effect of chloride activity (molality-based) and temperature on the repassivation potential of mill-annealed alloy 600

scattering range. Although the scattering of the data is substantial, both the data and the calculated curves show the same trends. For the 0·04%C alloy, the agreement is poorer in 0·001M solutions, since the experimental data indicate an increase in E_{rp} over the values for mill-annealed samples, whereas the model predictions do not show such an effect. The predictions obtained using only the grain boundary composition (thin lines) are, in general, lower than the data and provide a reasonable estimate of the lower limit of the repassivation potential. Predictions obtained using the unweighted averaging procedure are somewhat too high. While the weighted averaging procedure (thick lines) shows the best results, the predictions obtained from the alternative approaches are too close to draw unequivocal conclusions as to which procedure reflects the

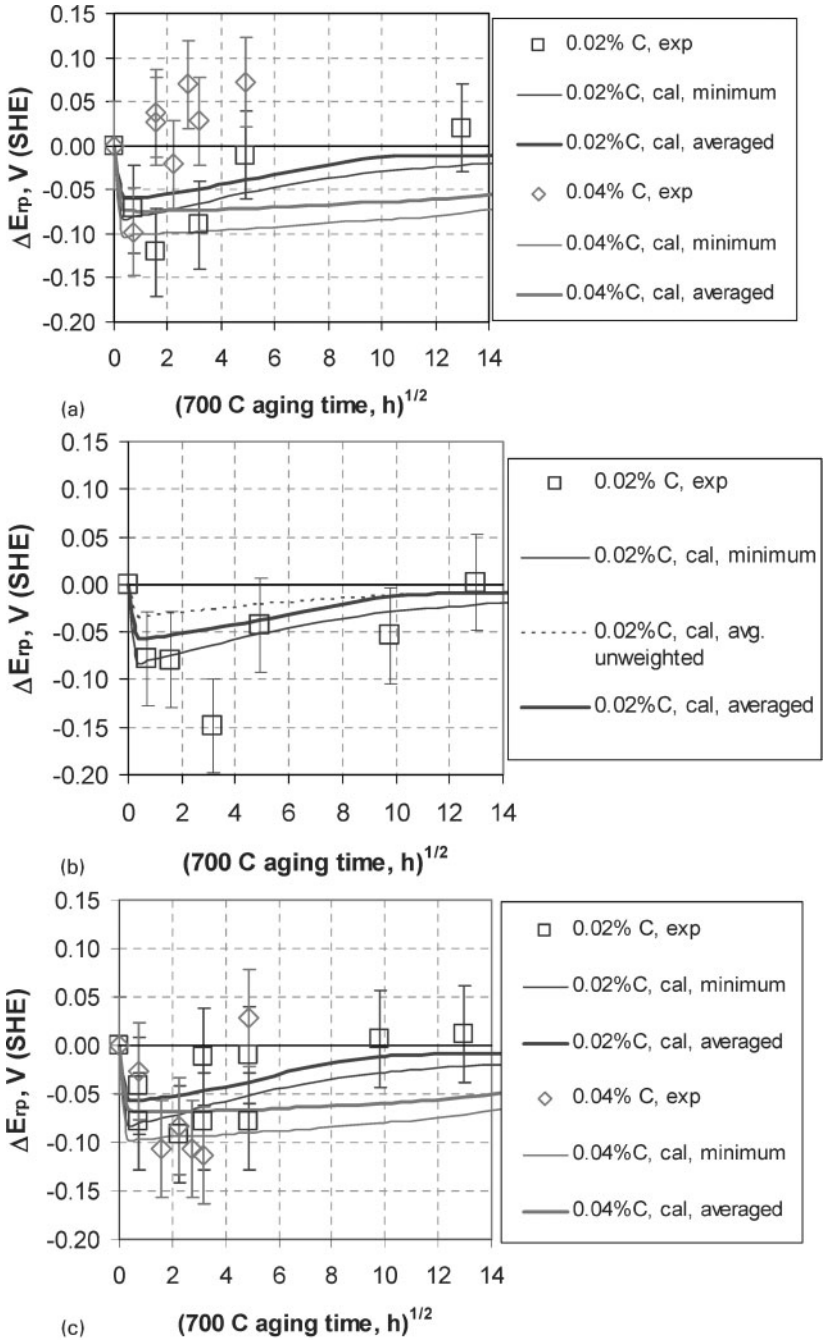

6 Predicted and experimental depression of the repassivation potential ($\Delta E_{rp}=E_{rp}-E_{rp,annealed}$) of alloy 600 heat-treated at 700°C. The repassivation potential was obtained at 60°C in *a* 0·001, *b* 0·005 and *c* 0·04M NaCl solutions

actual mechanism of localised corrosion stabilisation in alloy 600.

The repassivation potential initially drops fairly rapidly as a function of aging time and then slowly recovers towards the E_{rp} value of the annealed sample (which is indicated by the horizontal line in Fig. 6). This behaviour parallels the evolution of chromium depletion as a function of aging time. Although the calculated E_{rp} values can never exceed the repassivation potential of the bulk alloy, some of the experimental data lie above the horizontal line for $\Delta E_{rp}=0$. This apparently unphysical behaviour may be due to an incomplete homogenisation of the annealed samples, which may later proceed to completion as a result of the self-healing process. If the experimental points that lie above the $\Delta E_{rp}=0$ line are neglected, the lines calculated using the weighted averaging procedure are in reasonably good agreement with experimental data.

The depression of E_{rp} as a function of aging time is slightly deeper for the 0·04%C alloy compared with the 0·02% alloy, which reflects a lower concentration of chromium in the depleted zone of the alloy with a higher carbon content. This is illustrated in Fig. 7, which compares the predicted depletion profiles after 2·5 and 96 h of thermal aging for the 0·02 and 0·04%C lots. Furthermore, the higher carbon content has a substantial effect on the predicted recovery of the repassivation potential as a function of aging time, i.e. the recovery is notably slower for the alloy with a higher carbon content.

Results of calculations for alloy 825 are summarised in Figs. 8 and 9. In contrast to alloy 600, alloy 825

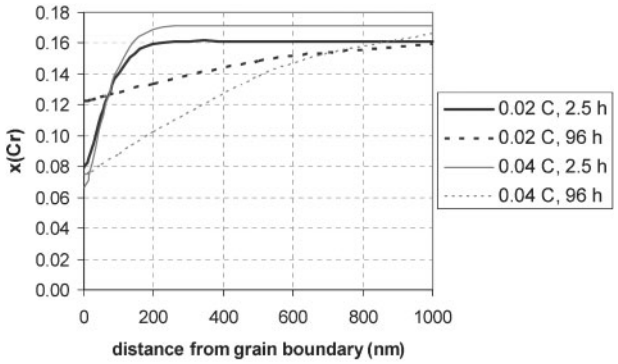

7 Predicted Cr depletion profiles for 0·02 and 0·04%C samples used for E_{rp} measurements[18] after heat treatment at 700°C

contains an appreciable amount of molybdenum. Therefore, the predicted repassivation potential depends on the molybdenum profile in addition to the chromium profile. To calculate molybdenum depletion, it has been assumed that the molar Mo/Cr ratio in the carbide (equation (35)) is the same as in the bulk alloy. This is consistent with measurements of grain boundary carbide compositions reported by Pan *et al.*[14]

The baseline results for the repassivation potential of mill-annealed alloy 825 are shown in Fig. 8 as a function of chloride ion activity and temperature.[19,46] The plot of E_{rp} versus chloride activity exhibits a change in slope, which is consistent with the repassivation potential model.[19] While the slope is low and similar to that observed for alloy 600 at higher chloride concentrations, it becomes much steeper in dilute solutions. This

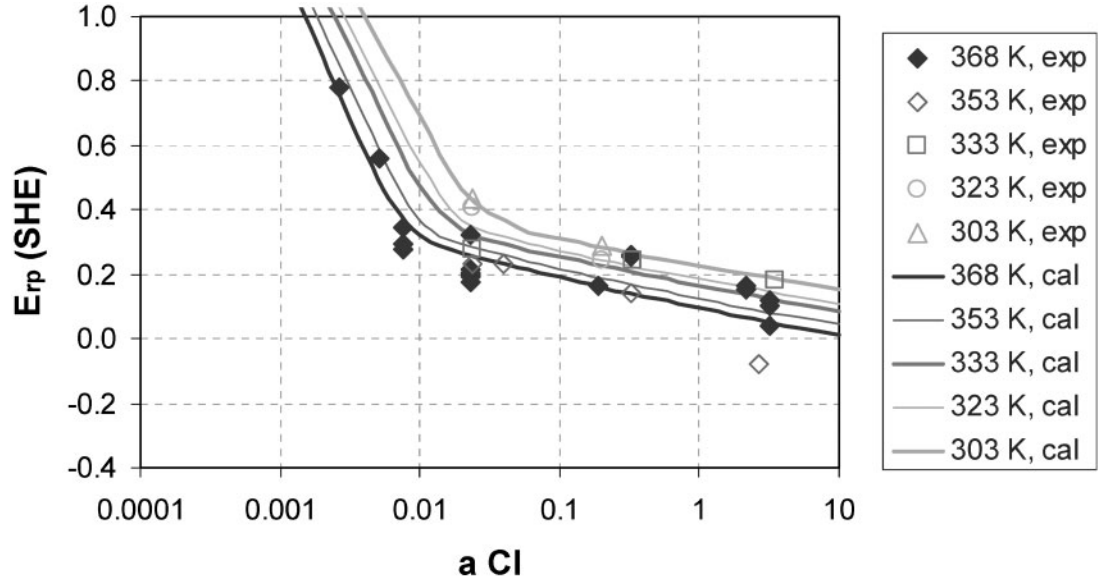

8 Effect of chloride activity (molality-based) and temperature on the repassivation potential of mill-annealed alloy 825. Experimental data are from Sridhar and Cragnolino[46] and Anderko *et al.*[19]

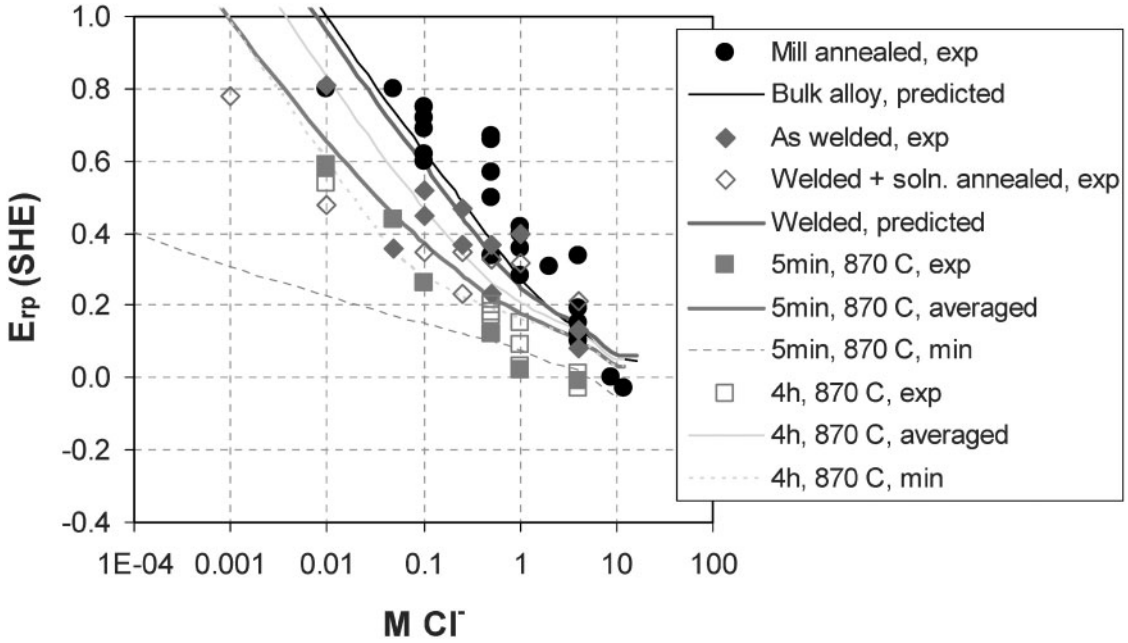

9 Predicted and experimental repassivation potential of alloy 22 as function of chloride concentration at 95°C in mill-annealed state, after welding and after welding followed by heat treatment at 870°C. Experimental data are from Dunn *et al.*[15–17]

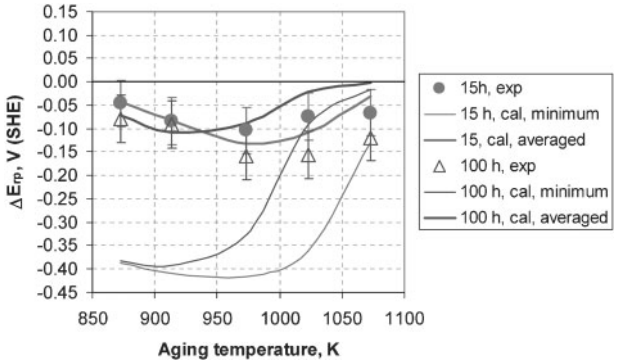

10 Predicted and experimental depression of repassivation potential ($\Delta E_{rp}=E_{rp}-E_{rp,annealed}$) of alloy 825 heat-treated at various temperatures. Repassivation potential was obtained at 95°C in 100 ppm (0·00282M) Cl^- solutions[14]

behaviour of E_{rp} as a function of chloride is common for corrosion-resistant alloys as discussed in previous studies.[19,24] As in Fig. 5, the lines have been obtained from the generalised correlation described in Appendix.

The E_{rp} measurements for thermally aged samples were performed at 95°C in 100 ppm (0·00282M) Cl^- solutions. These conditions are close to the transition between the high- and low-slope segments of the E_{rp} versus Cl activity plot, at which the repassivation potential is sensitive to environmental conditions. The calculated and experimental depression in the repassivation potential ΔE_{rp} is shown in Fig. 10 for samples aged for 15 and 100 h as a function of aging temperature. As with alloy 600, the calculations were performed using the averaging procedure (thick lines) and the grain boundary composition hypothesis (thin lines). In the case of alloy 825, the weighting factor $w(z)$ is always equal to 1 because the grain boundary concentration is always greater than the threshold concentration $x^*_{Cr}=0{\cdot}12$. Thus, the weighted averaging is equivalent to unweighted averaging here.

In contrast to alloy 600, the predicted minimum values of E_{rp} (thin lines) are much lower than the averaged values (thick lines). The predicted averaged values are in excellent agreement with experimental data for samples aged for 15 h (circles in Fig. 9). The comparison of the results obtained using both approaches provides a strong indication that the averaging procedure more accurately reflects the mechanism of localised corrosion stabilisation, which underscores the importance of a critical size. For the samples aged for 100 h, the agreement is good for lower aging temperatures, but the E_{rp} depression is underestimated for higher temperatures. However, the predicted ΔE_{rp} is consistent with the observed self-healing at higher temperatures after 100 h, which is indicated by the depletion profiles. Therefore, these deviations may be due to the incomplete self-healing of the samples used in the E_{rp} measurements.

Another indirect confirmation of the proposed methodology of averaging E_{rp} is provided by the cyclic potentiodynamic polarisation scans and potential staircase tests for sensitised samples of alloy 600.[18] These results indicate that there is no distinct two stage repassivation behaviour observed for sensitised alloys in either test. A hypothetical two-stage behaviour would support the notion that the repassivation of unsensitised areas is followed by the repassivation of the sensitised areas, which would reflect the minimum Cr/Mo composition. The fact that such behaviour is not observed is consistent with the assumption that the measured repassivation potential is an average over a relatively large area compared to the depletion zone. The measurements are likely to reflect the repassivation of a large pit that spans the grain boundary region, including some matrix.

Estimation of E_{rp} for welded Ni-based alloys

Modelling the alloy microchemistry in welded alloys is outside of the scope of this paper. However, the approach developed here for thermally aged alloys can be applied to welded alloys if the local composition of alloy components is available from experimental data or can be estimated. Then, the repassivation potential of welded samples can be estimated using the local composition information on the basis of the previously accepted assumption that E_{rp} primarily reflects the localised corrosion of the chromium and/or molybdenum-depleted regions.

It is known that solidification of nickel-based alloy welds leads to segregation patterns associated with dendrite formation.[47,48] The segregation leads to Ni depletion and solute (Cr, Mo, W) enrichment in interdendritic volumes. At the same time, the dendrite cores are somewhat depleted with respect to the solute components. Therefore, it is possible to estimate the repassivation potential on the basis of the dendrite core compositions. It should be noted that such an estimation does not explicitly take into account the effect of other phases that form as a result of solidification, in particular the topologically close-packed phases such μ, σ and P.[47–49] Although these phases are Mo-rich, it can be expected that the solute depletion is primarily due to segregation.

Figure 9 shows the calculated and experimental[16,17] repassivation potentials for mill-annealed and welded alloy 22. In both cases, E_{rp} was calculated from the correlation described in Appendix as a function of chloride activity. For the welded alloy, the composition of the dendrite core as reported by Cieslak *et al.*[47,48] has been assumed (i.e. Ni–20·0Cr–10·0Mo–2·7W–3·1Fe–0·006C–Ni). As shown in Fig. 9, the repassivation potential predicted for the welded sample is only slightly lower than that for the bulk alloy. These predictions are consistent with experimental data within their scattering range. Also, Fig. 9 includes the E_{rp} values that have been predicted for thermally aged welded samples using the procedures described above.

Discussion of model features

The microchemistry model described above is one-dimensional and assumes, in analogy with a number of previously published theories,[4,10,11,13,25,26,28–30] an effectively uniform carbide layer at the grain boundary. In reality, the continuity of the carbides depends on the aging treatment and may vary from continuous to widely spaced. A detailed treatment of discontinuous carbides would necessitate the use of a two-dimensional model, such as the collector plate model,[50,51] in which the size of carbides is explicitly taken into account and carbide growth is assumed to consist of volume diffusion

to the grain boundary, transport along the grain boundary to the precipitate and interfacial diffusion and deposition at the surface of the growing carbide. The collector plate model successfully reproduces the growth (i.e. lengthening and thickening) of grain boundary carbides[52,53] and has been applied, in conjunction with a finite difference numerical algorithm, to calculate two-dimensional Cr depletion profiles in the presence of discrete carbides.[27] However, the use of a two-dimensional microchemistry model was deemed unnecessary in the present study. First, the available experimental studies typically do not reveal a change in Cr content along the grain boundaries between discrete carbides, which is due to the much faster rate of grain boundary diffusion than the corresponding rate of bulk diffusion and indicates that the whole grain boundary acts as a collector plate to supply the precipitates with Cr.[54] In such cases, the Cr concentration is constant along the grain boundary, and the one-dimensional solution of Fick's law applies as described above even though the precipitates are discontinuous. In some partially sensitised grain boundaries, the carbides may be so widely spaced that the Cr diffusion fields around them may not overlap[7] and a two-dimensional model is necessary to fully reproduce the depletion profiles.[27] However, a one-dimensional model is still adequate in such cases to represent the Cr depletion in local areas around the carbides even though the distance over which carbon is withdrawn (equation (26)) may be then underestimated. Since localised corrosion is most likely to stabilise in the most susceptible, Cr-depleted areas, such a locally valid representation of Cr depletion should remain useful for estimating the repassivation potential (even though it may be less accurate for simulating intergranular corrosion). The second reason for not using a two-dimensional model here is due to the fact that it requires information about the spacing of carbides, which may change and is difficult to predict a priori. Third, a two-dimensional model is much more computationally demanding because it requires the numerical solution of differential equations rather than the semi-analytical solution derived here, which would make it cumbersome especially for repetitive calculations that are needed to evaluate E_{rp}. Thus, the one-dimensional model developed here can be expected to be sufficiently accurate for the purpose of modelling localised corrosion.

Additionally, it should be noted that a certain dispersion of results is expected to occur because of differences between various boundaries. The types of experiments that have been performed[14,18] to examine the effect of sensitisation on localised corrosion do not lend themselves to the examination of boundary-to-boundary differences. The scanning electrochemical techniques may be used to determine whether there are boundary-to-boundary differences in the electrochemical response, but these techniques are not useful for examining repassivation of pits along grain boundaries. It may be worthwhile to conduct, in the future, some studies on the effect of grain boundary mismatch on sensitisation and localised corrosion. Such studies would not negate the modelling approach that the dissolution rate at the bottom of pits is a function of local alloy chemistry: they would just add further complexity.

The model presented here does not take into account the effect of possible intragranular carbides. The formation of intragranular carbides would affect the mass balance of carbon and therefore, the depletion profiles would be changed primarily in the advanced healing regime. However, for the alloys considered here, there were few, if any, intragranular carbides for the aging treatments studied.[14] It is possible that under extreme aging conditions, intragranular precipitates may be observed, for example, on slip planes. Nevertheless, the approach presented here can be expected to remain valid even in the presence of some limited amount of intragranular carbides, since the mass balances are then not severely affected.

It is also of interest to examine how the results are affected by the carbon mass balance assumptions that have been made in the derivation of the depletion model. The assumption of the equality of carbon activity within the grain is unequivocally supported in the literature. This is due to the large difference between the diffusion coefficients of carbon and chromium or other substitutional elements. For example, the diffusion coefficient of C in austenite at 700°C [55] is $2{\cdot}2\times10^{-13}$ m^2 s^{-1} whereas that of Cr is $6{\cdot}8\times10^{-20}$ m^2 s^{-1} in type 304 stainless steel[56] or $1{\cdot}2\times10^{-19}$ in alloy 800.[57] Since the diffusion coefficients of C are about six orders of magnitude larger than those of Cr, the diffusion gradient of C is negligible compared to that of Cr at the same conditions. While the equality of carbon activity is generally accepted, the average distance d over which carbon can be withdrawn (equation (26)) is based on simple geometrical considerations[30] and requires an estimate of the average grain size. The healing of grain boundary depletion is affected by the parameter d. The healing occurs simultaneously with the gradual, thermodynamically driven depletion of carbon in the grain until carbon solubility is reached as described previously.[10] While the model described here qualitatively follows the grain carbon content evolution described by Was and Kruger,[10] Fig. 11 quantitatively illustrates the effect of the assumed grain size (equation (26)) on the depletion profiles. In Figure 11, calculations have been made for alloy 600 heat treated at 973 K for 1 and 100 h, assuming that the grain size varies in a very wide range from 30 to 500 μm. This range is wider than the commonly encountered range for nickel-based alloys. For short heat treatment times, the effect of the grain size is insignificant. On the other hand, it becomes important at long exposure times (e.g. 100 h in Fig. 11) for which healing plays a dominant role. As expected, healing occurs faster in small grains, in which carbon can be withdrawn rapidly from a small volume. It should be noted that the optimum grain sizes that provide the best representation of depletion profiles (Table 2) are reasonably close to experimental grain size estimates, when such estimates are available. This provides empirical support for the validity of equation (26). It is interesting to note that the grain size has a relatively limited effect on the calculated repassivation potential. This is due to the fact that, at the temperature–time conditions at which the grain size has a strong effect on depletion profiles (i.e. in the healing regime), the depletion profiles are relatively flat and, therefore, do not strongly contribute to the E_{rp} depression (which is most strongly affected by the lowest Cr/Mo concentrations). For example, the E_{rp} depression for alloy 600

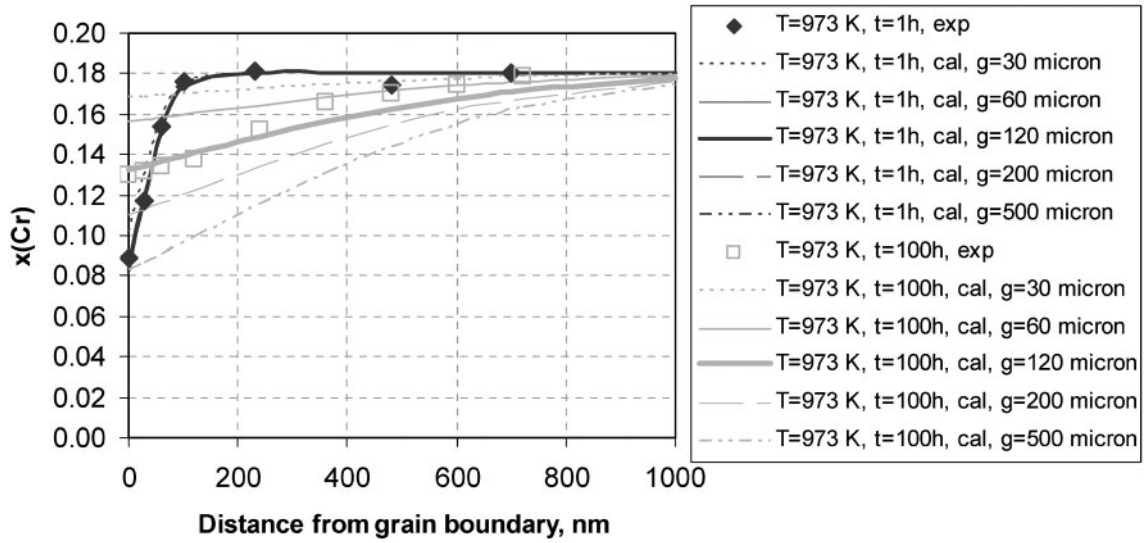

11 Effect of assumed grain size (ranging from 30 to 500 μm) on predicted Cr depletion profiles of alloy 600 heat treated at 973 K and 1 or 100 h. The experimental data of Was and Kruger[10] are shown for comparison

thermally aged at 973 K and 100 h (cf. Fig. 11) and exposed to 0·04 M NaCl solutions at 333 K ranges from −0·070 to −0·096 V for assumed grain sizes varying in a realistic range from 30 to 200 μm respectively.

Finally, it should be noted that the E_{rp} depression of austenitic alloys (both calculated and experimental) is relatively modest. Much larger depressions are observed for duplex alloys.[58] However, the mechanism of chromium depletion in duplex alloys is different and is outside of the scope of this study.

Conclusions

1. A general procedure has been developed for predicting the effect of thermal aging on the repassivation potential of austenitic alloys. The procedure combines two mechanistic models, a grain boundary microchemistry model for calculating the chromium and molybdenum depletion profiles in the vicinity of grain boundaries and an electrochemical model that relates the repassivation potential to alloy composition as well as temperature and solution chemistry.

2. The grain boundary microchemistry model combines a thermodynamic treatment of the paraequilibrium between grain boundary carbides and alloy matrix components with a closed-form solution for the diffusion of chromium and molybdenum. It accurately reproduces the experimental Cr and Mo depletion profiles for sensitised alloys 600, 825 and 316L. In addition to activity coefficients for the solid solution, the model utilises parameters that have a well-defined physical meaning, i.e. the composition and Gibbs energy of formation of the carbide phase, diffusion coefficients of Cr and Mo and average grain size. Thus, the model is applicable to alloys with different compositions, e.g. with different carbon contents.

3. Using the previously developed E_{rp} model, a methodology has been established to calculate the observable repassivation potential by integrating the E_{rp} values that correspond to the local alloy chemistry in the depletion zone. Such averaged values are in satisfactory agreement with experimental E_{rp} data that have been measured in chloride solutions for thermally aged samples of alloys 600 and 825.

4. In addition to the computation of the repassivation potential of thermally aged alloys, the model is applicable to alloys whose microchemistry has been altered by fabrication procedures. This has been demonstrated by estimating the repassivation potential of welded alloy 22.

Acknowledgements

The work reported here has been supported by the US Department of Energy (award no. DE-FC36-04GO14043) and co-sponsored by ChevronTexaco, DuPont, Haynes International, Mitsubishi Chemical, Shell and Toyo Engineering.

References

1. A. J. Sedriks: 'Corrosion of stainless steels'; 1996, New York, John Wiley & Sons.
2. S. Lamb (ed.): 'CASTI handbook of stainless steels and nickel-base alloys'; 2001, Edmonton, CASTI Publishing.
3. J. R. Davis (ed.): 'Corrosion of weldments'; 2006, Materials Park, OH, ASM International.
4. C. Stawström and M. Hillert: *J. Iron Steel Inst.*, 1969, **207**, 77–85.
5. C. S. Tedmon Jr., D. A. Vermilyea and J. H. Rosolowski: *J. Electrochem. Soc.*, 1969, **118**, 192–202.
6. V. Cihal: 'Intergranular corrosion of steels and alloys', Materials science monographs, Vol. 18; 1984, New York, Elsevier.
7. E. L. Hall and C. L. Briant: *Metall. Trans. A*, 1984, **15A**, 793–811.
8. E. L. Hall and C. L. Briant: *Metall. Trans. A*, 1985, **16A**, 1225–1236.
9. S. M. Bruemmer and L. A. Charlot: *Scr. Metall.*, 1986, **20**, 1019–1024.
10. G. S. Was and G. M. Kruger: *Acta Metall.*, 1985, **33**, 841–854.
11. G. S. Was: *Corrosion*, 1990, **46**, 319–330.
12. J. J. Kai, G. P. Yu, C. H. Tsai, M. N. Liu and S. C. Yao: *Metall. Trans. A*, 1989, **20A**, 2057–2067.
13. W. E. Mayo: *Mater. Sci. Eng. A*, 1997, **A232**, 129–139.
14. Y.-M. Pan, D. S. Dunn, G. A. Cragnolino and N. Sridhar: *Metall. Mater. Trans. A*, 2000, **31A**, 1163–1173.
15. D. S. Dunn, D. Daruwalla and Y.-M. Pan: 'Effect of fabrication processes on material stability – characterization and corrosion', Report CNWRA 2004-01, Southwest Research Institute, San Antonio, TX, USA, 2004.
16. D. S. Dunn, Y.-M. Pan, L. Yang and G. A. Cragnolino: *Corrosion*, 2006, **62**, 3–12.

17. D. S. Dunn, O. Pensado, Y.-M. Pan, R. T. Pabalan, L. Yang, X. He and K. T. Chiang: 'Passive and localized corrosion of alloy 22 – modeling and experiments', Report CNWRA 2005-02, Southwest Research Institute, San Antonio, TX, USA, 2005.
18. G. Tormoen, N. Sridhar and A. Anderko: *Corros. Eng. Sci. Technol.*, 2009, to be published.
19. A. Anderko, N. Sridhar and D. S. Dunn: *Corros. Sci.*, 2004, **46**, 1583–1612.
20. N. Sridhar, C. S. Brossia, D. S. Dunn and A. Anderko: *Corrosion*, 2004, **60**, 915–936.
21. D. S. Dunn, N. Sridhar, and G. A. Cragnolino: *Corrosion*, 1996, **52**, 115–124.
22. D. S. Dunn, G. A. Cragnolino and N. Sridhar: *Corrosion*, 2000, **56**, 90–104.
23. A. Anderko, N. Sridhar, L. T. Yang, S. L. Grise, B. J. Saldanha and M. H. Dorsey: *Corros. Eng. Sci. Technol.*, 2005, **40**, 33–42.
24. A. Anderko, N. Sridhar, M. A. Jakab and G. Tormoen: *Corros. Sci.*, 2008, **50**, 3629–3647.
25. R. L. Fullman: *Acta Metall.*, 1982, **30**, 1407–1415.
26. R. M. Kruger, G. S. Was, J. F. Mansfield and J. R. Martin: *Acta Metall.*, 1988, **36**, 3163–3176.
27. B. W. Bennett and H. W. Pickering: *Acta Metall.*, 1988, **36**, 539–546.
28. S. M. Bruemmer: *Corrosion*, 1990, **46**, 698–709.
29. H. Sahlaoui, H. Sidhom and J. Philibert: *Acta Mater.*, 2002, **50**, 1383–1392.
30. T. Sourmail, C. H. Too and H. K. D. H. Bhadeshia: *ISIJ Int.*, 2003, **43**, 1814–1820.
31. Y. F. Yin and R. G. Faulkner: *Corros. Sci.*, 2007, **49**, 2177–2197.
32. C. Zener: *J. Appl. Phys.*, 1949, **20**, 950–953.
33. R. E. Reed-Hill: 'Physical metallurgy principles', 3rd edn; 1991, Boston, MA, PWS-Kent Pub.
34. J. Crank: 'The mathematics of diffusion', 2nd edn; 1975, Oxford, Clarendon Press.
35. F. D. Richardson: *J. Iron Steel. Inst.*, 1953, **175**, 33–51.
36. S. S. Babu, in A. Anderko, P. Wang, R. D. Young, D. P. Riemer, P. McKenzie, M. M. Lencka, S. S. Babu and P. Angelini: 'Prediction of corrosion of alloys in mixed-solvent environments', Final report for the project DE-FC07-00CH11019, DOE Office of Industrial Technologies, June 2003, available at: http://www.osti.gov/servlets/purl/811533-wUOQwz/native/, subtask 1·1.
37. S. Hertzman: *Metall. Trans. A*, 1987, **18A**, 1753–1766.
38. S. Hertzman, *Metall. Trans. A*., 1987, **18A**, 1767–1778.
39. S. Hertzman and M. Jarl: *Metall. Trans. A*, 1987, **18A**, 1745–1752.
40. J.-O. Andersson and N. Lange: *Metall. Trans.*, 1988, **19A**, 1385–1394.
41. M. A. Gaudett and J. R. Scully: *J. Electrochem. Soc.*, 1993, **140**, 3425–3435.
42. X.-C. Jiang, T. Yoshimura, Y. Ishikawa, T. Shinohara and S. Tsujikawa: *J. Electrochem. Soc.*, 1992, **139**, 1001–1007.
43. G. S. Was, H. H. Tischner and R. M. Latanision: *Metall. Trans. A*, 1981, **12A**, 1397–1408
44. H. Sahlaoui, K. Makhlouf, H. Sidhom and J. Philibert: *Mater. Sci. Eng. A*, 2004, **A372**, 98–108.
45. A. Tekin, J. W. Martin and B. A. Senior: *J. Mater. Sci.*, 1991, **26**, 2458–2466.
46. N. Sridhar and G. A. Cragnolino: *Corrosion*, 1993, **49**, 885–894.
47. M. J. Cieslak, T. J. Headley and A. D. Romig: *Metall. Trans. A*, 1986, **17A**, 2035–2047.
48. M. J. Cieslak, G. A. Knorovsky, T. J. Headley and A. D. Romig, Jr.: *Metall. Trans. A*, 1986, **17A**, 2107–2116.
49. H. M. Tawancy: *J. Mater. Sci.*, 1996, **31**, 3929–3936.
50. H. B. Aaron and H. I. Aaronson: *Acta Metall.*, 1968, **16**, 789–798.
51. A. D. Brailsford and H. B. Aaron: *J. Appl. Phys.*, 1969, **40**, 1702–1710.
52. J. Caisley and R. G. Faulkner: *Met. Sci.*, 1977, **11**, 200–207.
53. R. A. Carolan and R. G. Faulkner: *Acta Metall.*, 1988, **36**, 257–266.
54. T. Thorvaldsson and G. L. Dunlop: *J. Mater. Sci.*, 1983, **18**, 793–803.
55. P. Thibaux, A. Métenier and C. Xhoffer: *Metall. Mater. Trans. A*, 2007, **38A**, 1169–1176.
56. T. Thorvaldsen and A. Salwén: *Scr. Metall.*, 1984, **18**, 739–742.
57. A. R. Paul, K. N. G. Kaimal, M. C. Naik and S. R. Dharwadkar: *J. Nucl. Mater.*, 1994, **217**, 75–81.
58. T. Amadou, A. Ben Rhouma, H. Sidhom, C. Braham and J. Ledion: *Metall. Mater. Trans. A*, 2000, **31A**, 2015–2024.

Appendix

Generalised correlation for predicting the repassivation potential

The E_{rp} model has been described in detail and validated against experimental data in previous papers[19,24] and therefore, only the final equations are summarised here. In a general case of a system containing NA aggressive ions and NI inhibitive ions, the repassivation potential E_{rp} is obtained by solving an equation given by

$$1+\sum_{k}^{NI}\left[\left(\frac{i_{rp}}{i_p}-1\right)\frac{l''_k}{i_{rp}}\right]\theta_k^{n_k}\exp\left(\frac{\xi_k F E_{rp}}{RT}\right)= \sum_{j}^{NA}\frac{k''_j}{i_{rp}}\theta_j^{n_j}\exp\left(\frac{\alpha_j F E_{rp}}{RT}\right) \quad (51)$$

where i_p is the passive current density, i_{rp} is the current density threshold that defines repassivation ($i_{rp}=10^{-2}$ A m^{-2}), θ_j is the partial surface coverage fraction by solution species j, T is the temperature, R is the gas constant, F is the Faraday constant and k''_j, l''_k, n_j, n_k, α_j and ξ_k are electrochemical kinetic parameters as defined below. The summation on the right-hand side of equation (51) is performed over all aggressive species (j=1, 2, …, NA), and the summation on the left-hand side pertains to inhibitive species (k=1, 2, …, NI). The H_2O molecules are treated as inhibitive species because they contribute to the formation of the oxide layer. The electrochemical parameters of the model are defined as follows:

(i) the quantity k''_j is the reaction rate constant for alloy dissolution mediated by the adsorption of aggressive species j. This constant is used in a scaled form (i.e. as $k_j=k''_j/i_{rp}$) and is expressed using a scaled Gibbs energy of activation $\Delta g^{\neq}_{A,j}$

$$k_j=\frac{k''_j}{i_{rp}}=\exp\left(-\frac{\Delta g^{\neq}_{A,j}}{RT}\right) \quad (52)$$

(ii) the quantity l''_k is the reaction rate constant for the formation of oxide mediated by the adsorption of inhibitive species k. It is also used in a scaled form, i.e. as

$$l_k=\left(\frac{i_{rp}}{i_p}-1\right)\frac{l''_k}{i_{rp}}$$

and is expressed using a scaled Gibbs energy of activation $\Delta g^{\neq}_{Ik}$

$$l_k=\left(\frac{i_{rp}}{i_p}-1\right)\frac{l''_k}{i_{rp}}=\exp\left(-\frac{\Delta g^{\neq}_{I,k}}{RT}\right) \quad (53)$$

(iii) The quantities n_j and n_k are the reaction rate orders with respect to the aggressive species j and inhibitive species k respectively

(iv) The parameters α_j and ξ_k are the electrochemical transfer coefficients for the reactions involving the aggressive species j and inhibitive species k respectively. The parameter α_j has been assumed to be equal to one for simplicity.

Since the model has a limiting character, it has been shown[19] that the partial coverage fraction of a species j

can be related to the activity of this species in the bulk solution through an adsorption isotherm, i.e.

$$\theta_j = \frac{r_j a_j}{1 + \sum_k r_k a_k} \tag{54}$$

where the adsorption coefficient is defined using the Gibbs energy of adsorption $\Delta G_{ads,i}$, i.e.

$$r_j = \exp\left(-\frac{\Delta G_{ads,j}}{RT}\right) \tag{55}$$

For H_2O in aqueous solutions, θ_{H_2O} is assumed to be equal to one for simplicity. For calculating the temperature dependence of the kinetic parameters, the scaled Gibbs energies of activation are further related to temperature as

$$\frac{\Delta g^{\neq}_{A,j}}{T} = \frac{\Delta g^{\neq}_{A,j}(T_{ref})}{T_{ref}} + \Delta h^{\neq}_{A,j}\left(\frac{1}{T} - \frac{1}{T_{ref}}\right) \tag{56}$$

for aggressive ions and

$$\frac{\Delta g^{\neq}_{I,k}}{T} = \frac{\Delta g^{\neq}_{I,k}(T_{ref})}{T_{ref}} + \Delta h^{\neq}_{I,k}\left(\frac{1}{T} - \frac{1}{T_{ref}}\right) \tag{57}$$

for water and inhibitive species. In equations (56) and (57), the parameters $\Delta g^{\neq}_{A,j}(T_{ref})$ and $\Delta g^{\neq}_{I,j}(T_{ref})$ are the scaled Gibbs energies of activation at reference temperature T_{ref}=298·15 K for the reactions mediated by the adsorption of aggressive and inhibitive ions respectively. The quantities $\Delta h^{\neq}_{A,j}$ and $\Delta h^{\neq}_{I,k}$ are the corresponding enthalpies of activation.

The environments considered in this study are limited to one kind of aggressive species (i.e. the Cl^- ions) and one kind of inhibitive species (i.e. the H_2O molecules). In such a case, the repassivation potential is characterised, in the most general case, by seven parameters, i.e. $\Delta g^{\neq}_{A,Cl}(T_{ref})$ $\Delta h^{\neq}_{A,Cl}$, $n_{A,Cl}$, $\Delta g^{\neq}_{I,H_2O}(T_{ref})$, $\Delta h^{\neq}_{I,H_2O}$, ξ_{I,H_2O}, and $\Delta G_{ads,Cl}$. In a previous study,[24] generalised expressions for these parameters have been developed. Specifically, the Gibbs energy of adsorption of ions $\Delta G_{ads,Cl}$, the electrochemical transfer coefficient for the formation of passive oxide as a result of a reaction with water ξ_{I,H_2O} and the reaction order with respect to Cl^- ions $n_{A,Cl}$ have been set equal to common values, i.e.

$$\Delta G_{ads,Cl}/(\text{kJ/mol}) = 10 \tag{58}$$

$$\xi_{I,H_2O} = 0{\cdot}8 \tag{59}$$

$$n_{A,Cl} = 1{\cdot}1 \tag{60}$$

The enthalpies of activation $\Delta h^{\neq}_{A,Cl}$ and $\Delta h^{\neq}_{I,H_2O}$ (in kJ mol^{-1}) have been found to be linearly related to the respective Gibbs energies of activation $\Delta g^{\neq}_{A,Cl}(T_{ref})$ and $\Delta g^{\neq}_{I,H_2O}(T_{ref})$, i.e.

$$\Delta h^{\neq}_{A,Cl} = 55 + 2\Delta g^{\neq}_{A,Cl}(T_{ref}) \tag{61}$$

$$\Delta h^{\neq}_{I,H_2O} = -15 + 32\Delta g^{\neq}_{I,H_2O}(T_{ref}) \tag{62}$$

Finally, the two Gibbs energies of activation $\Delta g^{\neq}_{A,Cl}(T_{ref})$ and $\Delta g^{\neq}_{I,H_2O}(T_{ref})$ have been expressed in terms of alloy composition for Fe–Ni–Cr–Mo–W–N alloys. The Gibbs energy of activation (in kJ mol^{-1}) for dissolution mediated by adsorption of aggressive species $\left[\Delta g^{\neq}_{A,Cl}(T_{ref})\right]$ is calculated as a sum of four contributions, i.e.

$$\Delta g^{\neq}_{A,Cl}(T_{ref}) = \Delta g^{\neq}_{A,Cl}(Cr,Fe,Ni) + \Delta g^{\neq}_{A,Cl}(Mo,W) + \Delta g^{\neq}_{A,Cl}(N) + \Delta g^{\neq}_{A,Cl}(misc) \tag{63}$$

where $\Delta g^{\neq}_{A,Cl}(Cr,Fe,Ni)$ is the baseline contribution for Fe–Ni–Cr alloys, $\Delta g^{\neq}_{A,Cl}(Mo,W)$ is an increment due to the effect of Mo and W, $\Delta g^{\neq}_{A,Cl}(N)$ is an increment due to N and $\Delta g^{\neq}_{A,Cl}(misc)$ is a miscellaneous contribution of other elements. The baseline contribution for Fe–Ni–Cr alloys is given by

$$\Delta g^{\neq}_{A,Cl}(Cr,Fe,Ni) = \Delta g^{\neq}_{A,Cl}(Fe)w_{Fe} + \Delta g^{\neq}_{A,Cl}(Ni)w_{Ni} + 398{\cdot}5w_{Cr}w_{Ni}^{0{\cdot}7} + 555{\cdot}9w_{Cr}w_{Fe}^{0{\cdot}7} - 335{\cdot}4w_{Cr} \tag{64}$$

where $\Delta g^{\neq}_{A,Cl}(Fe) = -74{\cdot}1$ and $\Delta g^{\neq}_{A,Cl}(Ni) = -18{\cdot}7$ are the Gibbs energies of activation for iron (or, for practical purposes, carbon steel) and nickel respectively. The remaining contributions are calculated as

$$\Delta g^{\neq}_{A,Cl}(Mo,W) = w_{Cr}(w_{Mo} + w_W)^{0{\cdot}4}(893{\cdot}9w_{Ni}^{1{\cdot}7} + 839{\cdot}0w_{Fe}^{1{\cdot}7}) \tag{65}$$

$$\Delta g^{\neq}_{A,Cl}(N) = w_N^{0{\cdot}5}w_{Cr}^{3}(-1{\cdot}293e5w_{Fe}^{0{\cdot}2} + 1{\cdot}451e5w_{Ni}^{0{\cdot}2}) \tag{66}$$

$$\Delta g^{\neq}_{A,Cl}(misc) = -1764w_{Nb}w_{Cr} \tag{67}$$

With the current database, the $\Delta g^{\neq}_{A,Cl}(misc)$ term is limited to the effect of Nb and should be treated as tentative. An expression similar to equation (63) has been adopted for the Gibbs energy of activation for the formation of oxide mediated by adsorption of H_2O, i.e.

$$\Delta g^{\neq}_{I,H_2O}(T_{ref}) = \Delta g^{\neq}_{I,H_2O}(Cr,Fe,Ni) + \Delta g^{\neq}_{I,H_2O}(Mo,W) + \Delta g^{\neq}_{I,H_2O}(N) + \Delta g^{\neq}_{I,H_2O}(misc) \tag{68}$$

where

$$\Delta g^{\neq}_{I,H_2O}(Cr,Fe,Ni) = 18{\cdot}14w_{Fe} + 169{\cdot}6w_{Ni} + 1983w_{Cr}^{1{\cdot}1} \tag{69}$$

$$\Delta g^{\neq}_{I,H_2O}(Mo,W) = -2422\left[(w_{Mo} + w_W)^{1{\cdot}1} + w_{Cr}^{1{\cdot}1}(w_{Fe} + 1{\cdot}4w_{Ni})\right] + 2024\left[(w_{Mo} + w_W)^{1{\cdot}1}(w_{Fe}^{0{\cdot}5} + w_{Ni}^{0{\cdot}5})\right] \tag{70}$$

$$\Delta g^{\neq}_{I,H_2O}(N) = w_N^{0{\cdot}5}w_{Cr}^{3}\left[-2{\cdot}607d5w_{Fe}^{0{\cdot}2} + 2{\cdot}384e5w_{Ni}^{0{\cdot}2}\right] \tag{71}$$

$$\Delta g^{\neq}_{I,H_2O}(misc) = -4950w_{Nb}w_{Cr} \tag{72}$$

Equations (51)–(72) constitute a generalised correlation for predicting E_{rp} of Fe–Ni–Cr–Mo–W–N alloys as a function of composition. The overall average deviation between the calculated results and experimental data for all alloys is 67 mV.[24] The effect of ions other than Cl^- can be also included as discussed in a previous study,[24] but such ions are outside of the scope of this work.